Diffusion-Tensor MR Imaging and Tractography: Exploring Brain Microstructure and Connectivity[1]

Paolo G. P. Nucifora, MD, PhD
Ragini Verma, PhD
Seung-Koo Lee, MD, PhD
Elias R. Melhem, MD, PhD

Diffusion magnetic resonance (MR) imaging is evolving into a potent tool in the examination of the central nervous system. Although it is often used for the detection of acute ischemia, evaluation of directionality in a diffusion measurement can be useful in white matter, which demonstrates strong diffusion anisotropy. Techniques such as diffusion-tensor imaging offer a glimpse into brain microstructure at a scale that is not easily accessible with other modalities, in some cases improving the detection and characterization of white matter abnormalities. Diffusion MR tractography offers an overall view of brain anatomy, including the degree of connectivity between different regions of the brain. However, optimal utilization of the wide range of data provided with directional diffusion MR measurements requires careful attention to acquisition and postprocessing. This article will review the principles of diffusion contrast and anisotropy, as well as clinical applications in psychiatric, developmental, neurodegenerative, neoplastic, demyelinating, and other types of disease.

[1] From the Department of Radiology, Sections of Neuroradiology (P.G.P.N., E.R.M.) and Biomedical Image Analysis (R.V.), Hospital of the University of Pennsylvania, 3400 Spruce St, Philadelphia, PA 19104; and Department of Diagnostic Radiology and Research Institute of Radiological Science, Yonsei University College of Medicine, Seoul, Korea (S.K.L.). Received March 14, 2006; revision requested May 18; revision received November 10; accepted December 18; final version accepted February 12, 2007; final review by E.R.M. May 17. **Address correspondence to** E.R.M. (e-mail: *emelhem@rad.upenn.edu*).

Radiology

Described by Le Bihan et al (1) in 1986, diffusion-weighted (DW) imaging has rapidly been adopted into the radiologic armamentarium. The most common application is the early detection of ischemia, as manifested by restricted diffusion in a territorial distribution (2). Clinically, DW imaging is nearly ideal for this purpose: It is highly sensitive, highly specific, and noninvasive and provides a diagnosis within the therapeutic window (3). However, the scope of diffusion imaging extends beyond the detection of acute ischemia. By incorporating directionality into a DW measurement, diffusion-tensor (DT) images can be obtained. Rather than probe cellular pathophysiology, DT imaging provides a means of investigating tissue microstructure and brain anatomy. This article will review the principles of diffusion contrast and anisotropy, as well as clinical applications in psychiatric, developmental, neurodegenerative, neoplastic, demyelinating, and other types of disease.

Principles

Diffusion contrast is based on the self-diffusion of water molecules in tissue (1,4). Although a variety of sequences are now used to acquire DW images, all DW sequences include two equal and opposing motion-probing gradients. As a result of being subjected to opposing gradients, the signal from a voxel will decrease exponentially as a function of the strength of the gradients *(G)*, the duration of the gradients (Δ), the amount of time passing between the gradients (δ), and the diffusion coefficient of water molecules in the voxel *(D)*. The first three factors do not vary from voxel to voxel and can be quantified collectively with a *b* value, defined as $\gamma^2G^2\delta^2(\Delta - \delta/3)$, where γ is the gyromagnetic constant. Only intravoxel diffusion *(D)* varies from voxel to voxel, and thus contrast in a DW image is a function of the apparent diffusion coefficient. The relative contributions of T2 contrast and diffusion contrast in the DW signal *(S)* are governed by the Stejskal-Tanner equation, $S = S_0 \times e^{-bD}$, where S_0 is the signal measured without motion-probing gradients that is used to form the image with a *b* value of 0 sec/mm^2 (hereafter, *b*0 image).

DW imaging is only sensitive for motion of water molecules that is aligned with the motion-probing gradients. In gray matter, changing the direction of the gradient does not substantially affect the signal since diffusion is roughly isotropic (equally likely in all directions). On the other hand, diffusion in white matter is often strongly anisotropic and occurs maximally in the same orientation as white matter tracts (Fig 1) (5). Anisotropic diffusion is an effect of the microstructural properties of the voxel, and decreased anisotropy is a common feature of neuronal abnormalities. The relationship between tissue microstructure and anisotropy is probably multifactorial: Evidence is mounting for the hypothesis that the integrity of the myelin sheath and axonal membrane is reflected by restriction of diffusion orthogonal to the fiber, whereas the integrity of intra-axonal structures (such as microtubules) is positively correlated with diffusion parallel to the fiber (6–12). However, anisotropy may also be decreased from nonspecific abnormalities such as vasogenic edema.

The tensor model was developed to characterize diffusion in anisotropic voxels, where it cannot be represented by a single value due to its directional dependence. Several measures may be derived from a tensor. For example, a three-dimensional principal eigenvector indicates the direction of greatest diffusion within a voxel. Likewise, scalar (directionless) eigenvalues signify the magnitude of the diffusivities along the principal eigenvector and two orthogonal minor eigenvectors.

In the tensor model, it is assumed that a water molecule undergoing diffusion for a limited time will generally be constrained to a volume known as the diffusion ellipsoid. This volume is spherical in voxels with isotropic diffusion, where water diffusion is completely symmetric. In contrast, voxels with anisotropic diffusion have oblate (flattened) or prolate (elongated) diffusion ellipsoids, depending on the relative magnitudes of the eigenvalues. Although it is possible to produce an image that represents the diffusion ellipsoid in every voxel, interpreting such an image is cumbersome. For this reason, properties of the tensor are often abstracted by various indices to produce gray-scale or color maps. For example, the trace is a simple index of diffusion determined by the sum of the principal diffusivities. Similarly, fractional anisotropy (FA) is an index ranging from 0 (isotropic) to 1 (maximally anisotropic) and is defined as by using the following equation:

$$FA = \sqrt{\frac{2}{3}} \cdot \sqrt{\frac{(\lambda_1 - \bar{\lambda})^2 + (\lambda_2 - \bar{\lambda})^2 + (\lambda_3 - \bar{\lambda})^2}{\lambda_1^2 + \lambda_2^2 + \lambda_3^2}}$$

for eigenvalues λ_1, λ_2, and λ_3 and mean diffusivity $\bar{\lambda}$. Anisotropy maps are often color encoded to represent directional

Essentials

- Diffusion-tensor (DT) imaging is capable of demonstrating abnormalities in a variety of disorders, ranging from multiple sclerosis to neurodegenerative disease, potentially with higher sensitivity and specificity than conventional imaging.
- The emerging field of clinical tractography is poised to make substantial contributions to preoperative planning in neuro-oncology and epilepsy.
- Those who are armed with a sound understanding of the principles of DT imaging and tractography will likely find DT imaging to be a useful tool in investigating the relationships between structure and function in the brain.

Published online
10.1148/radiol.2452060445

Radiology 2007; 245:367–384

Abbreviations:
BOLD = blood oxygen level–dependent
DT = diffusion tensor
DW = diffusion weighted
FOV = field of view
ROI = region of interest

Authors stated no financial relationship to disclose.

information regarding the principal eigenvector (Fig 2). Taken together, a combination of these maps provides a useful compromise between ease of interpretation and clinical utility. Even at low resolution, they can be used to segment white matter tracts by visual inspection, thus allowing a radiologist to evaluate "white-white" contrast.

Acquisition

To construct a map of apparent diffusion coefficients, images must be obtained by using at least two *b* values. Typically, a DW image with a *b* value ranging from 700 to 1200 sec/mm^2 is used with an accompanying *b*0 image (13–17). The diffusivity trace map is derived from the three principal diffusivities and requires four measurements: a *b*0 image and DW images with motion-probing gradients applied in three orthogonal directions (14). To produce anisotropy maps or perform tractography, the full tensor must be determined for each voxel. In theory, this can be accomplished by using *b*0 image and DW images acquired with six different motion-probing gradients. In practice, however, more than six DW images are often obtained to improve reliability, either by repeating the acquisition or by using additional motion-probing gradients. The optimal number of motion-probing gradients and their orientation are under debate, but diffusion-encoding schemes making use of 12 or more motion-probing gradients are not unusual (14,18,19).

The signal from tissue that undergoes gross motion may be misinterpreted as increased diffusivity, therefore scan times are generally kept short by using large voxel sizes and fast acquisition techniques such as echo-planar imaging (20). However, DT imaging with spin-echo echo-planar imaging and (less commonly used) gradient-echo echo-planar imaging is associated with several forms of artifacts. Some, such as eddy current distortion, are amenable to correction during postprocessing and can further be reduced with a modified acquisition (21–27). Likewise, artifacts induced with cardiac pulsation can be decreased with cardiac gating (28). Cerebrospinal fluid, which has a very high apparent diffusion coefficient, can contaminate measurements in nearby voxels; this can be addressed by decreasing voxel size or using fluid-attenuated inversion-recovery DW imaging (29–33).

On the other hand, susceptibility artifact at air-bone interfaces in the skull is more difficult to correct. Single-shot

Figure 1

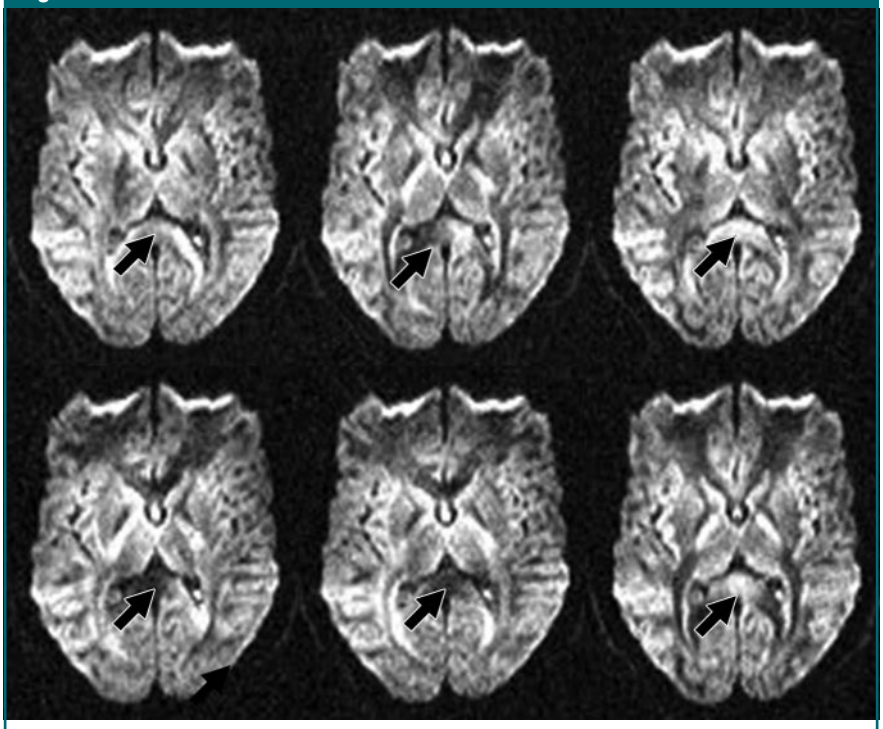

Figure 1: Multiple transverse DW images (*b* value, 800 sec/mm^2; repetition time msec/echo time msec, 6500/99; matrix, 128 × 128; field of view [FOV], 220 × 220 mm; section thickness, 3 mm) of same brain slice with diffusion gradients applied in different directions demonstrate anisotropic diffusion. Signal intensity of white matter varies with direction of diffusion gradients, most conspicuously in corpus callosum (arrows). Signal is strongest when diffusion gradient is oriented orthogonally to white matter fiber tracts, as in two panels on right.

Figure 2

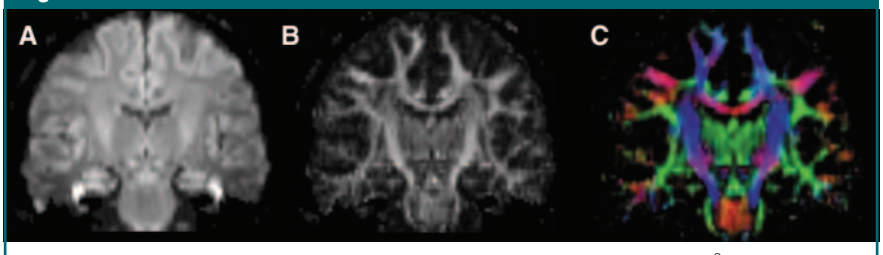

Figure 2: Common types of coronal DT images (12 directions; *b* value, 800 sec/mm^2; 6500/99; matrix, 128 × 128; FOV, 220 × 220 mm; section thickness, 3 mm) in a healthy subject. *A,* Mean diffusivity maps, *B,* fractional anisotropy maps, and *C,* color-encoded maps of the principal eigenvector (red, left to right; blue, cranial to caudal; green, anterior to posterior).

Figure 3

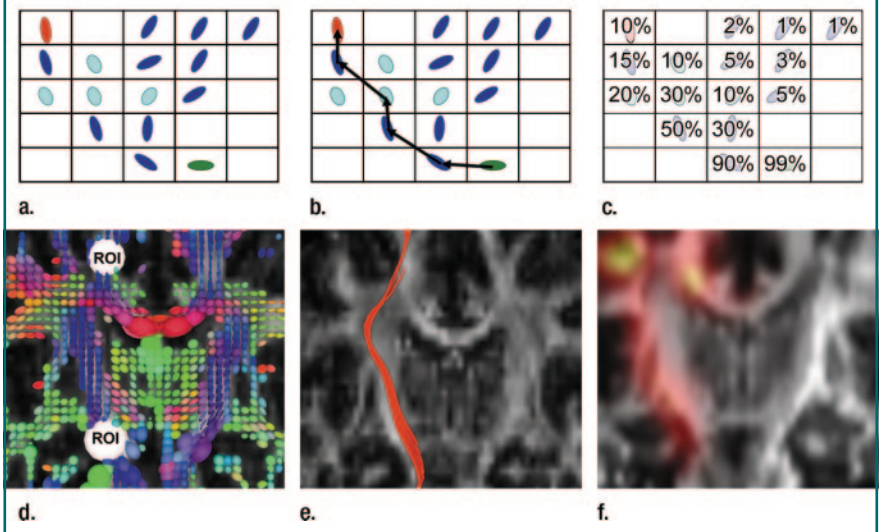

Figure 3: **(a)** Abstract representation of tensors in a 5 × 5 grid, with two regions of interest (ROIs) (red and green). Strongly anisotropic voxels are dark blue, whereas weakly anisotropic voxels are light blue. **(b)** Streamline tractography propagates a fiber tract in the direction of principal eigenvector, preserving voxel-to-voxel directional information. **(c)** Probabilistic tractography produces a likelihood map of the diffusion path between two ROIs. Rather then delineate a single best path, the likelihood map shows the probability that a particle diffusing between ROIs traverses each voxel. Coronal images of internal capsule in healthy adults demonstrate **(d)** diffusion ellipsoid maps (principal eigenvector is denoted by color: red, left to right; blue, cranial to caudal; green, anterior to posterior), **(e)** streamline tractography of corticospinal tract (red), and **(f)** probabilistic tractography of corticospinal tract (color denotes index of probability that voxel is included in tract) (12 directions; *b* value, 800 sec/mm^2; 6500/99; matrix, 128 × 128; FOV, 220 × 220 mm; section thickness, 3 mm).

Figure 4

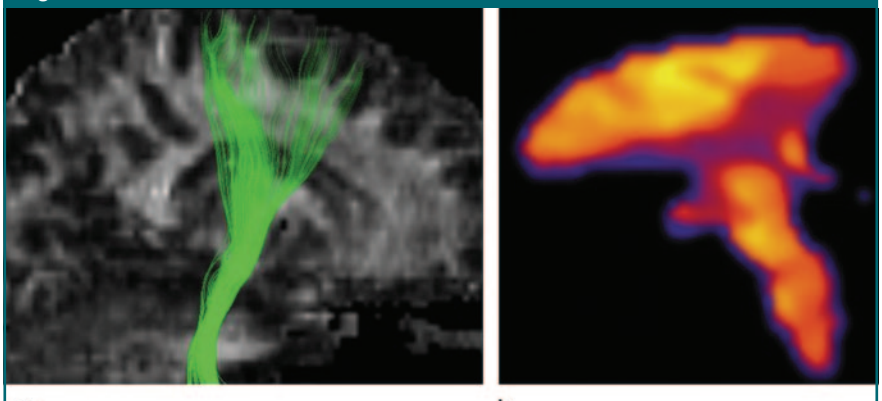

Figure 4: **(a)** Tractography of corticospinal tract performed by iteratively extending streamlines (green) from a seed ROI in the direction of principal eigenvector by using the fiber assignment by continuous tracking, or FACT, algorithm (63,64). Images are superimposed on sagittal fractional anisotropy map. **(b)** Volume-rendered probability map of corticospinal tract produced by generating several thousand tracts from each seed voxel (69). Rather than follow the same path, since each track is extended it may overlap or depart from the rest at random. The probability of deviating from principal eigenvector in a traversed voxel reflects its diffusion properties, with increased divergence in voxels of low anisotropy. Probability map is formed from superposition of all tracts from all voxels in the seed ROI tract (color denotes index of probability that voxel is included in tract) (DT imaging: 12 directions; *b* value, 800 sec/mm^2; 6500/99; matrix, 128 × 128; FOV, 220 × 220 mm; section thickness, 3 mm).

stimulated-echo acquisition mode, or STEAM, MR imaging has shown promise in reducing susceptibility artifact (34). Several multi-shot diffusion protocols have also been used to reduce susceptibility artifact without introducing phase errors from subject motion (35). For example, line-scan imaging is relatively insensitive to motion, and although used mainly in the spine, it has also been applied to DT imaging of the brain (36,37). Alternately, navigator information can be acquired during a multi-shot sequence to account for motion during reconstruction. One such approach is periodically rotated overlapping parallel lines with enhanced reconstruction, or PROPELLER, DT imaging, which acquires data in a rotating blade of k-space (38–40). Similarly, self-navigated interleaved spiral, or SNAILS, DT imaging acquires data through a spiral in k-space (41). In both cases, the oversampled center of k-space provides the navigator data. Finally, parallel imaging has proved useful in reducing susceptibility artifact in both single-shot and multi-shot acquisitions (42–44).

Although the tensor model can represent most white matter regions, it does not adequately describe voxels with crossing, diverging, or converging white matter tracts (45–47). These fiber

Figure 5

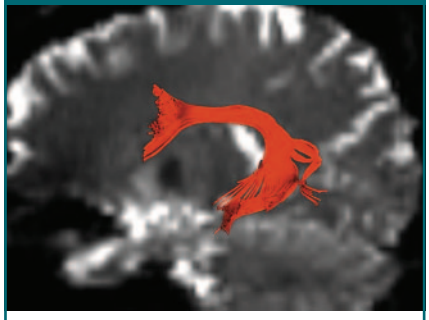

Figure 5: Tractography (12 directions; *b* value, 800 sec/mm^2; 6500/99; matrix, 128 × 128; FOV, 220 × 220 mm; section thickness, 3 mm) of a healthy right-handed subject demonstrates frontotemporal fiber tracts corresponding to arcuate fasciculus (red), superimposed on a sagittal *b* 0 image. This white matter tract connects motor and receptive speech centers and has greater relative fiber density in the left hemisphere.

tracts theoretically could be resolved with improved voxel resolution, perhaps by using high-field-strength imaging (48). Presently, however, multiple directions of diffusion within a single voxel are modeled with higher order vectors (49–51). Higher order methods generally involve examining q-space, which contains the Fourier transform of diffusion properties just as k-space in conventional MR imaging contains the Fourier transform of magnetic properties (52–54). DT imaging is based on a very limited sampling of q-space, and the resulting ellipsoids rely on several assumptions regarding the properties of diffusion in a voxel (49,55). High angular resolution diffusion imaging, or HARDI, methods, while more time consuming than DT imaging, use increased sampling in q-space to produce an improved diffusion profile (49,56–58). Diffusion spectrum imaging, for example, uses data throughout all of q-space to reconstruct a complete diffusion profile (50,59). In contrast, q-ball imaging samples points that are arranged on the surface of a sphere in q-space, reducing acquisition times by focusing on the diffusion parameters that are most relevant to tractography. Q-space techniques have proved useful in resolving multiple white matter orientations in regions such as the centrum semiovale, where DT imaging generally performs poorly (60–62). However, their steeper technical requirements have limited their clinical use.

Once fiber orientations have been determined for a sufficient number of voxels, tractography can be used to draw inferences regarding the overall geometry of white matter in the brain. A wide variety of algorithms are used for this purpose (Fig 3). Generally, streamline (deterministic) tractography connects neighboring voxels by propagating the ends of fiber tracts from user-defined seed voxels until termination criteria are met, such as excessive angular deviation of the fiber tracts or subthreshold voxel anisotropy (46,63–68). Although the seed voxels define the origin of all fiber tracts under examination, additional regions may be designated to restrict the output to a tract of interest.

Figure 6

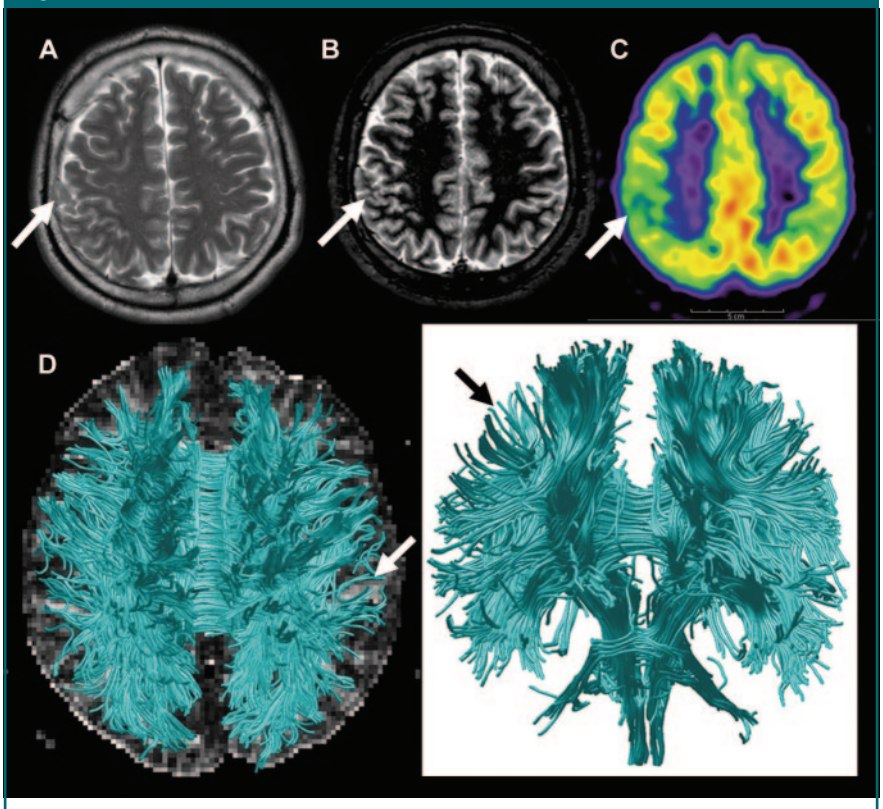

Figure 6: Images in 17-year-old boy with left-side motor seizure. *A,* Equivocal finding (arrow) on transverse T2-weighted image(4000/100; matrix, 352 × 352; FOV, 230 × 230 mm; section thickness, 5 mm). *B,* Transverse fast inversion recovery with myelin suppression image (repetition time msec/echo time msec/inversion time msec, 4500/22/300; section thickness, 3 mm; matrix, 256 × 256; FOV, 230 × 230 mm) shows focal cortical dysplasia in right precentral gyrus (arrow). *C,* Transverse fluorine 18 fluorodeoxyglucose positron emission tomography reveals decreased metabolism in right precentral area. *D,* Whole-brain white matter tractography (blue-green) depicts decreased subcortical fiber connectivity in right precentral area and adjacent cortex (DT imaging: 32 directions; six-channel sensitivity encoding; sensitivity encoding factor of two; *b* value, 600 sec/mm^2; 6599 – 8280/70; matrix, 96 × 96; FOV, 220 × 220 mm; section thickness, 2.3 mm).

For instance, tractography of the corticospinal tract may include fiber tracts if and only if they pass through both the internal capsule and the cerebral peduncles (Fig 3a). Tract selection and seed placement are typically highly interactive, which can result in strong operator dependence.

Other algorithms emphasize quantification of the probability of connection between two points, sometimes omitting the linear structures generated in streamline tractography (Fig 3b) (69,70). To improve the depiction of regions of fiber crossing, tractography algorithms have been developed that propagate a wavefront of varying size rather than a line, allowing fiber tracts to diverge and recombine (61,71–73). Probabilistic (distributed) tractography produces a global map that may be analyzed independently from other DT imaging measures; the value of each voxel in the map is the likelihood that the voxel is included in the diffusion path between two ROIs (Fig 4). Probabilistic methods are especially useful for tracking through regions of lower anisotropy, including gray matter (69).

Although tractography corresponds well to classic neuroanatomy, it is vexed by the problem of validation: the degree

Figure 7

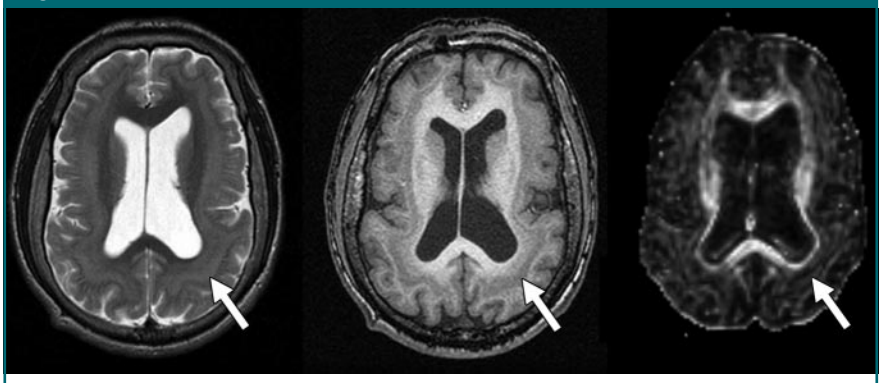

Figure 7: Images in 18-year-old woman with band heterotopia. Transverse T2-weighted (left) (4000/100; matrix, 352 × 352; FOV, 230 × 230 mm; section thickness, 5 mm) and T1-weighted (middle) (450/12; matrix, 256 × 256; FOV, 230 × 230 mm; section thickness, 5 mm) images demonstrate thick band heterotopia (arrow) with homogeneous signal intensity to gray matter, a so-called double cortex. This band shows high anisotropy (arrow) on fractional anisotropy map (right), suggesting its radial orientation and arrested neuronal migration (32 directions; six-channel sensitivity encoding; sensitivity encoding factor of two; *b* value, 600 sec/mm^2; 6599–8280/70; matrix, 96 × 96; FOV, 220 × 220 mm; section thickness, 2.3 mm). It is also consistent with passage of intact white matter tracts through the abnormality.

Figure 8

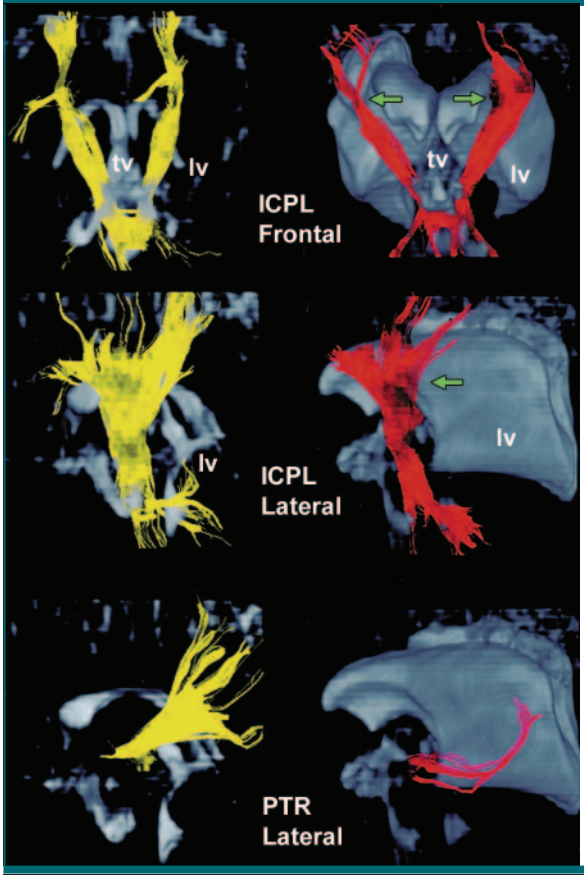

Figure 8: Tractography in patient with periventricular leukomalacia demonstrates degeneration of posterior thalamic radiation *(PTR)*, with intact fiber tracts (arrows) in the posterior limb of internal capsule *(ICPL)* (six directions; *b* value, 600 sec/mm^2; 5000–6000/92; matrix, 64 × 51; FOV, 120 × 96 mm; section thickness, 3 mm). *lv* = lateral ventricle, *tv* = third ventricle. (Reprinted, with permission, from reference 131.)

to which its results differ from those of anatomic methods such as dissection (75). A one-to-one correspondence would be optimal, as tractography could then serve as a substitute for other methods. But even divergence between tractography and traditional anatomic methods would not necessarily diminish its utility; if its findings in disease are reproducible, then tractography evidently measures something that varies according to pathologic features and therefore may be valuable. Thus, it is encouraging to find that tractography has properties appropriate to useful clinical and research tools, such as high interobserver and intraobserver reliability (76,77).

Analysis

DT imaging produces numerous measures ranging in dimension from scalars to tensor fields, which calls for a wide variety of statistical techniques to perform group analyses. Specific methods for the statistical analysis of full tensors remain under development (78,79). Currently, scalar DT imaging measures (including but not limited to anisotropy, diffusivity, and probability maps) are most commonly compared by using histogram, ROI, or voxel-based analysis. To establish confidence intervals in these measures, bootstrap methods repeatedly sample data from multiple acquisitions (80–83).

Histogram analysis does not require any presuppositions regarding anatomy or pathologic features, making it suitable for widespread diseases such as multiple sclerosis or small vessel ischemic disease (74,84–86). The brain is considered globally, and the frequencies of particular DT imaging values in different individuals are evaluated. Consequently, only global conclusions can be drawn regarding the composition of white and/or gray matter, which may be a disadvantage when considering lesions in the brain, as their effects are often dependent on location.

ROI analysis is used to test hypotheses regarding specific regions where disease is suspected. If motor symptoms are present, for example, DT imaging

measures may be calculated only in voxels believed to contain the internal capsule. Any significant differences that are detected can be ascribed to the ROI, thus offering a possible correlation between structure and function. Potential pitfalls include bias in ROI selection, which can partially be addressed by automation (87–90). In addition, ROIs drawn on DT images may suffer from artifact and decreased resolution, whereas those drawn on higher resolution images must be accurately registered to the DT images. Intersubject registration can be used to reduce error by standardizing ROIs on every subject. However, registration of full tensor datasets must be performed carefully; in registered tensor maps, unlike scalar maps, corresponding voxels do not have the same values since the operations used to map voxels during registration should change the orientation of the tensors. For instance, a shear deformation should cause tensors to realign in the direction of the shear. Thus, conventional registration should be followed by proper reorientation of tensors (91–93).

Finally, DT imaging measures can be compared on a voxel-by-voxel basis to localize differences between groups without a priori assumptions regarding the location of pathologic features (although voxels near each other are often assumed to be correlated to mitigate the problem of multiple comparisons) (94). Voxel-based analysis is usually less operator dependent and more easily automated than ROI analysis, but it can only be performed after intersubject registration (91–93). Statistical packages originally developed for blood oxygen level–dependent (BOLD) functional MR imaging have been adopted for DT imaging measures, including scalar maps of anisotropy and diffusivity (95). Nevertheless, it is important to be aware of the limitations of these methods when interpreting results, particularly when statistically significant voxels or clusters are detected that do not have a reasonable anatomic correlate (96,97).

Tractography is still in its infancy, and no consensus has emerged regarding the best means of analyzing its output. It is often used to segment white matter into specific tracts; the corpus callosum, for example, has been segmented according to the cortical destination of its fiber tracts, with correlation of callosal lesions to clinical presentation (98,99). One of the more promising methods of analysis is to examine a DT imaging measure such as anisotropy along the course of a selected fiber tract, which can either be performed during tractography or by defining a specific reference frame afterward (100–102). Finally, probabilistic tractography has been used to generate a connectivity matrix describing the relationships between every pair of voxels; by examining patterns within the matrix, clusters of white matter with homogeneous connectivity can be determined (103). It is important to bear in mind that trac-

Figure 9

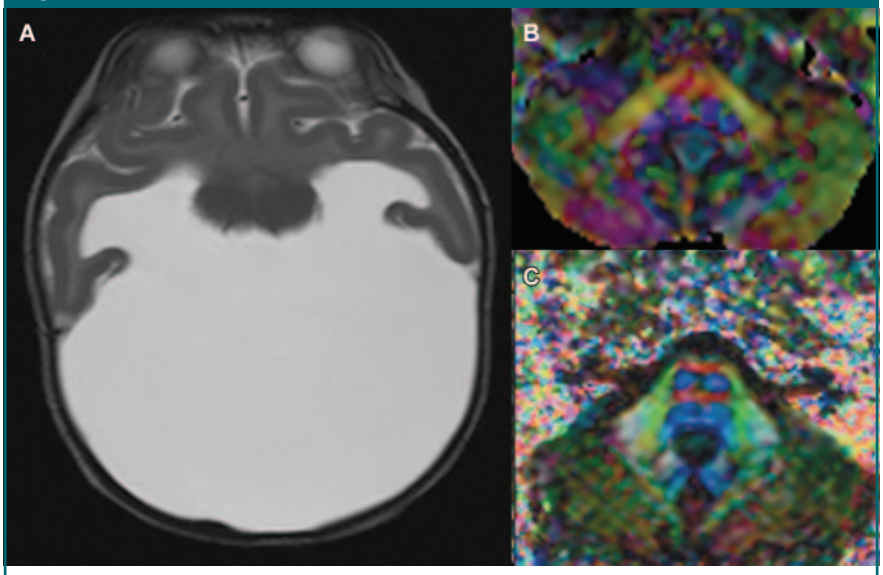

Figure 9: A, Transverse T2-weighted image (3000/20, 80) demonstrates alobar holoprosencephaly. *B,* Transverse color-encoded DT image depicts absence of corticospinal tracts (red, left to right; blue, cranial to caudal; green, anterior to posterior). C, Transverse color-encoded DT image depicts normal corticospinal tracts in healthy subject (DT imaging: six directions; *b* value, 600 sec/mm^2; 5000–6000/92; matrix, 64 × 64; FOV, 120 × 120 mm; section thickness, 3 mm). (Reprinted, with permission, from reference 133.)

Figure 10

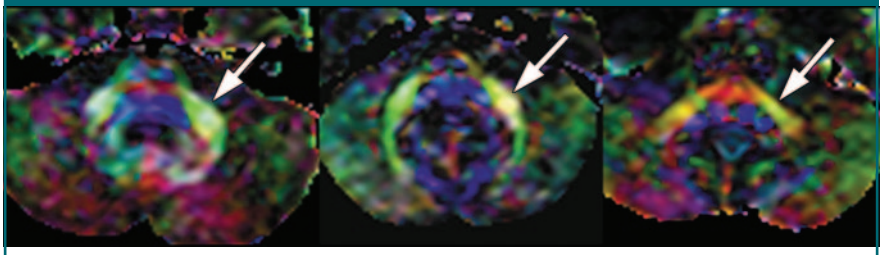

Figure 10: Transverse color-encoded DT images (red, left to right; blue, cranial to caudal; green, anterior to posterior) of middle cerebellar peduncle (arrows) in patients with alobar (right), semilobar (middle), and lobar (left) holoprosencephaly demonstrate manifestation of increasing severity of holoprosencephaly (six directions; *b* value, 600 sec/mm^2; 5000–6000/92; matrix, 64 × 64; FOV, 120 × 120 mm; section thickness, 3 mm). (Reprinted, with permission, from reference 133.)

tography findings can be affected by any process that alters diffusion anisotropy, including those external to the axon such as vasogenic edema. Thus, interpretation of tractography requires an appreciation of the distinction between anatomy and physiology.

Applications

Normal Brain

All of these types of analyses have been used to demonstrate the relationship between white matter structure and function. For example, IQ has been positively correlated with anisotropy in white matter association tracts (104). Reading ability has been correlated with anisotropy of the left temporoparietal white matter, where tractography has localized the white matter circuitry connecting Broca and Wernicke language areas (Fig 5) (105–110). In visual pathways, increased anisotropy has been correlated with improved reaction time, and tractography can be used to demonstrate topographically ordered fiber tracts in normal subjects (intriguingly, these fiber tracts are disorganized in the blind) (111–114).

Tractography findings have shown excellent correlation with functional data. For example, probabilistic tractography has been used for segmentation of the thalamus according to its cortical connectivity, which corresponds well to segmentation of the thalamus at BOLD functional MR imaging (69,115). Likewise, probabilistic tractography of the medial frontal cortex has demonstrated an anatomic boundary that corresponds to the functional boundary between supplemental motor cortex and presupplemental motor cortex (103). Throughout the brain, regions with similar tractographic features tend to be functionally co-activated, informally validating the axiom that "neurons that fire together, wire together" (103,115,116).

Figure 11

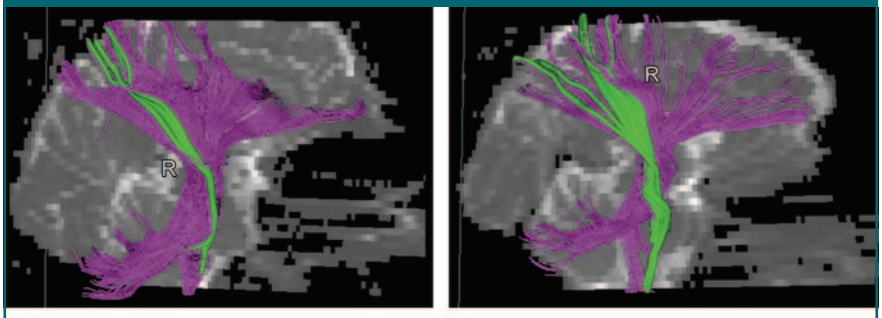

Figure 11: Tractography (12 directions; *b* value, 800 sec/mm^2; 6500/99; matrix, 128 × 128; FOV, 220 × 220 mm; section thickness, 3 mm) in **(a)** a patient with amyotrophic lateral sclerosis and **(b)** a healthy subject. Tractography is superimposed on sagittal *b*0 image. In the right *(R)* hemisphere, descending fiber tracts connecting the cortex and brainstem are shown in purple and the corticospinal tract is shown in green. The ratio of the number of fiber tracts in corticospinal tract to the total number fiber tracts is decreased in amyotrophic lateral sclerosis. (Reprinted, with permission, from reference 145.)

Figure 12

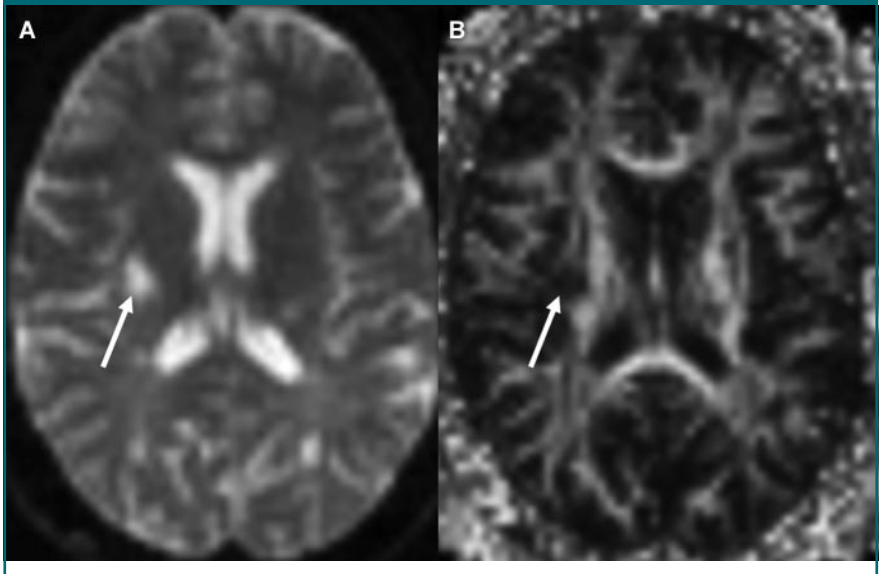

Figure 12: *A,* Transverse *b*0 image demonstrates focus of signal abnormality (arrow) in the right corona radiata in 38-year-old woman with multiple sclerosis. *B,* Transverse fractional anisotropy map of lesion (arrow) demonstrates decreased anisotropy (DT imaging: 12 directions; *b* value, 800 sec/mm^2; 6500/99; matrix, 128 × 128; FOV, 220 × 220 mm; section thickness, 3 mm).

Developmental Abnormalities

In premature newborns, increased anisotropy is found in developing cortical gray matter rather than in unmyelinated white matter, and cortical anisotropy steadily decreases during the first few months of life (99,117–125). This likely reflects the radial anisotropy of the glial scaffolding that guides the migration of neurons to the cortex (126,127). Unsurprisingly, a spectrum of migrational abnormalities and other developmental brain disorders has been demonstrated with DT imaging. For example, DT imaging has identified cortical dysplasia with greater sensitivity than did conventional MR imaging (Fig 6) (128). In patients with band heterotopias, tractography has been used to suggest potential connectivity between regions of heterotopic gray matter and normal cortex

(Fig 7) (129). In lissencephaly, tractography of the grossly abnormal subcortical and deep white matter has demonstrated incomplete development of the fornix and cingulate tracts (130). Tractography in patients with periventricular leukomalacia has supported the hypothesis that spastic paralysis may involve extrapyramidal and sensory pathways (Fig 8) (131,132). DT imaging in patients with alobar holoprosencephaly has demonstrated absent corticospinal tracts (Fig 9) (133). Many white matter tract structures, such as the middle cerebellar peduncles, were found to be smaller in alobar holoprosencephaly than in semilobar holoprosencephaly or lobar holoprosencephaly (Fig 10). Furthermore, the size of the corticospinal tracts and middle cerebellar peduncles in all three variants was correlated with neurodevelopmental status.

Aging and Neurodegenerative Disease

Although mild decreases in anisotropy are a normal result of aging, DT imaging has shown additional abnormalities in patients with several types of dementia and neurodegenerative disease (134–137). For example, a study of patients with early Parkinson disease demonstrated decreased anisotropy in the substantia nigra but normal anisotropy in the putamen and caudate nucleus (138). Increased diffusivity and decreased anisotropy were found in the corpus callosum and the frontal, temporal, and parietal white matter in both patients with Alzheimer disease and those with Lewy body dementia, but the occipital lobes were involved only in the latter—possibly reflecting the greater incidence of visual hallucinations in Lewy body dementia (139–141). Asymptomatic carriers of apolipoprotein E ε4, a susceptibility marker for Alzheimer disease, demonstrated abnormal diffusivity and decreased anisotropy in the parahippocampal white matter, a finding that may be valuable in early diagnosis (142). Likewise, DT imaging in patients with asymptomatic Huntington disease demonstrated decreased anisotropy in several regions of white matter (143). Finally, multiple groups have demonstrated decreased anisotropy and increased diffusivity in the internal capsule and cerebral peduncles of patients with amyotrophic lateral sclerosis (Fig 11) (144–151). Throughout the corticospinal tract, anisotropy decreased as amyotrophic lateral sclerosis progressed, and decreased anisotropy was correlated with slowed nerve conduction time (152–154).

Figure 13

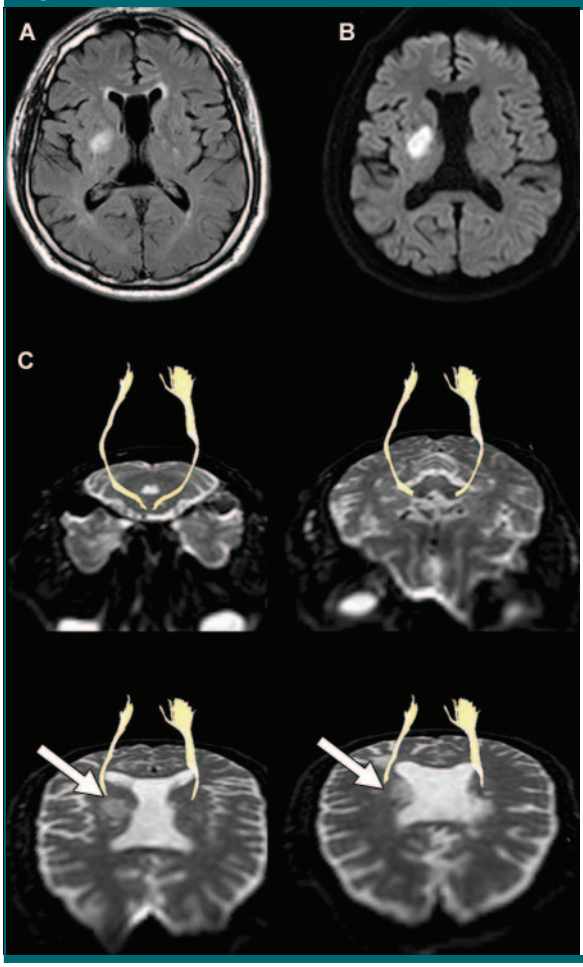

Figure 13: Images in 55-year-old man who complained of sudden onset of left-sided weakness. Transverse, *A,* fluid-attenuated inversion-recovery (9000/90/2000; matrix, 288 × 288; FOV, 230 × 230 mm; section thickness, 5 mm) and, *B,* DW (six directions; six-channel sensitivity encoding; sensitivity encoding factor of two; *b* value, 1000 sec/mm^2; 3300/60; matrix, 128 × 128; FOV, 230 × 230 mm; section thickness, 5 mm) images show acute infarction in right basal ganglia. *C,* Fiber tractography with superimposed transverse *b*0 image (32 directions, six-channel sensitivity encoding; sensitivity encoding factor of two; *b* value, 600 sec/mm^2; 6599–8280/70; matrix, 96 × 96; FOV, 220 × 220 mm; section thickness, 2.3 mm) clearly shows the relationship between infarction and corticospinal tract. The infarct is anterior to the course of corticospinal tract (arrows). The patient experienced complete recovery of motor function.

Psychiatric Disease

Since schizophrenia may involve disordered brain connectivity, many investigators have used DT imaging to demonstrate a variety of white matter abnormalities, often correlated with performance on neuropsychiatric tests (155–163). For example, decreased anisotropy in the white matter subserving language centers has been correlated with the presence of auditory hallucinations (160). However, a consensus has not yet emerged regarding the appearance of schizophrenia by using DT imaging, possibly due to differences in methods (96,164–166). Nevertheless, DT imaging continues to be used in psychiatric illnesses with suspected disruption of brain connectivity. For example, decreased anisotropy has been described in the arcuate fasciculus of children with behavior disorders, in the prefrontal white matter of patients with bipolar disorder, and in the right superior frontal gyrus of elderly patients with depression (167–169). Moreover, several regions of white matter demonstrate abnormal anisotropy in children with attention deficit disorder, obsessive-compulsive disorder, and autism (170–172). Finally, decreased anisotropy in the corpus callosum has been

demonstrated in ethanol dependence and may also be a trait of cocaine dependence (173,174).

Demyelinating Disease

The specificity of DT imaging measures for white matter abnormalities has spurred its use in demyelinating diseases, particularly multiple sclerosis. Several groups have demonstrated increased diffusivity and decreased anisotropy in demyelinating lesions (Fig 12) (175–179). In some studies, diffusivity and anisotropy varied with the degree and type of contrast enhancement (177,179,180). However, DT imaging has also demonstrated abnormalities in normal-appearing white matter and normal-appearing gray matter; it is unclear whether the latter represents an inflammatory lesion in gray matter or the effects of retrograde axonal degeneration (181–183). Patients with primary or secondary progressive multiple sclerosis demonstrated increased gray matter diffusivity, compared with patients with relapsing-remitting multiple sclerosis or healthy controls (184). In patients with clinically isolated syndromes (considered a precursor to multiple sclerosis), tractography has defined the corticospinal tracts and demonstrated higher lesion volume within them than in other white matter, although the correlation between disease progression and DT findings is less concrete (185).

Figure 14

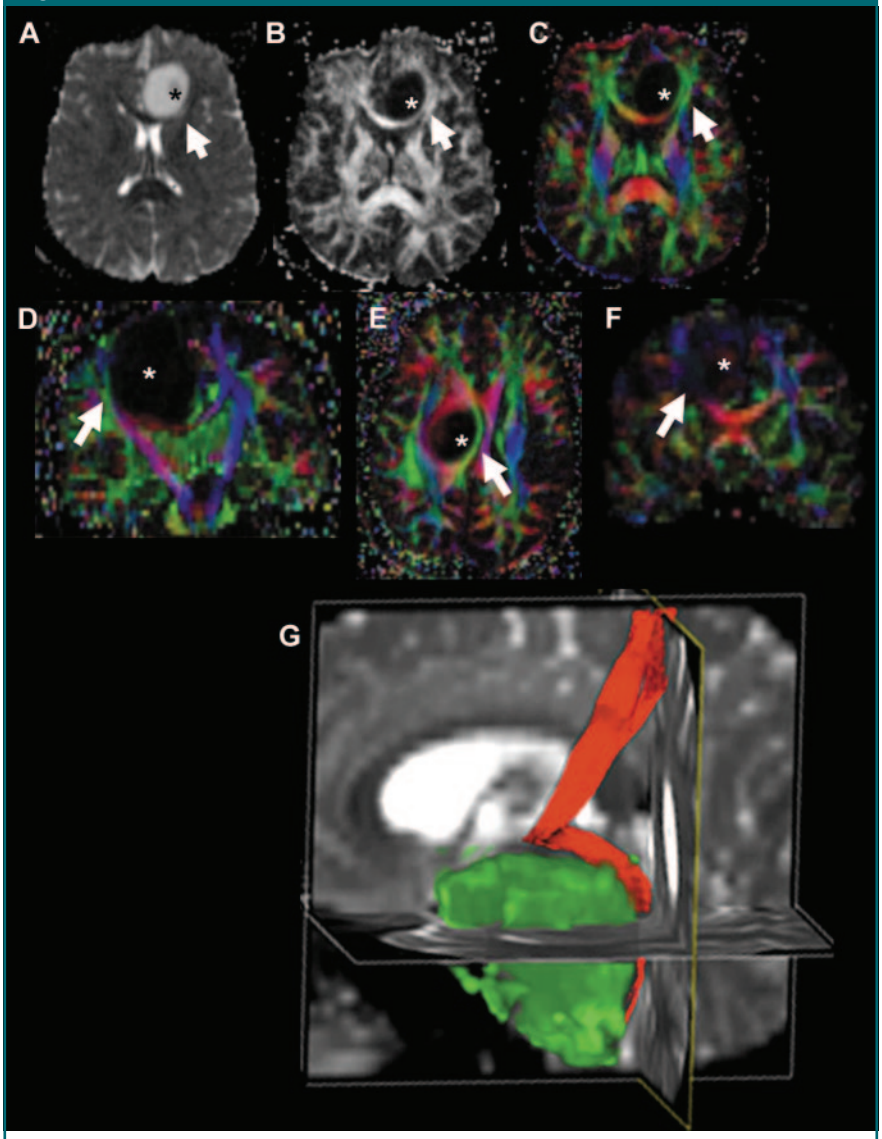

Figure 14: Transverse *(A–C, E)* and coronal *(D, F)* color-encoded DT images (red, left to right; blue, cranial to caudal; green, anterior to posterior) demonstrate displacement *(A–C)*, infiltration *(D–E)*, and destruction *(F)* of white matter tracts (arrow) by tumor (*). *G*, Tractography with superimposed sagittal *b* 0 image demonstrates displacement of white matter tracts (red) by tumor (green) (12 directions; *b* value, 800 sec/mm^2; 6500/99; matrix, 128 × 128; FOV, 220 × 220 mm; section thickness, 3 mm).

Ischemic Disease

The use of diffusion imaging in ischemic disease is expanding well beyond its proved role in detection of early acute ischemia into the domain of prognosis and long-term management of ischemic sequelae. Initial uses of tractography in stroke have demonstrated involvement of sensorimotor pathways by acute ischemic insults with strong correspondence to clinical symptoms (Fig 13) (186–191). Tractography has also demonstrated anatomic reorganization of language pathways after an ischemic insult, concordant with BOLD functional MR findings of reorganized language activation (192). Finally, patients with cerebral autosomal dominant arteriopathy with subcortical infarcts and leukoencephalopathy, or CADASIL, syndrome demonstrated decreased anisotropy and increased diffusivity in normal-appearing white matter, likely representing early ischemia. Interestingly, DT imaging abnormalities in the frontal lobes and cingulate fasciculus have been associated with specific types of cognitive impairment in this disease (193,194).

Neoplasms

As well as improving sensitivity, DT imaging may also play a role in improving specificity, particularly in radiologically ambiguous lesions such as T2 hyperintense peritumoral voxels. Hyperintense white matter voxels surrounding gliomas, which presumably were partly tu-

mor infiltrated, demonstrated lower anisotropy than did hyperintense white matter voxels of equal diffusivity surrounding metastases and meningiomas, which presumably were merely edematous (195–198). This may have important implications in the delineation of tumor margins beyond what is currently demonstrated with conventional imaging (199,200). Eventually, changes in the diffusivity pattern of a tumor might be used to predict tumor response to chemotherapy and radiation (201,202).

As neurosurgeons increasingly consider the degree to which tumors may displace and disrupt white matter tracts (Fig 14), the anatomic guidance provided by tractography is emerging as an important part of preoperative planning (203–205). This is particularly true of eloquent white matter such as the corticospinal tract, where tractography has been a useful adjunct to intraoperative fiber stimulation (206–208). Preoperative tractography showing tumor involvement of the corticospinal tract has been correlated to motor deficits, even when motor cortex was uninvolved (209). Conversely, normalization at postoperative tractography was predictive of improvement in function, suggesting a role for intraoperative tractography (210,211). For inoperable tumors, tractography may be helpful in gamma knife planning, and it has already been used in the radiosurgical treatment of arteriovascular malformations (212).

Epilepsy

Neurosurgical uses for tractography are not limited to oncology; there are multiple examples of the use of tractography in surgical planning for epilepsy (Fig 15). Intraoperative maps of language centers in epilepsy have been analyzed with tractography to suggest locations of eloquent white matter (213). Tractography has also been used to determine whether seizure foci involved the visual radiations, and findings were concordant with cortical visual evoked potentials (214). Likewise, probabilistic tractography of the Meyer loop in epilepsy was performed with sufficient accuracy to predict visual field

Figure 15

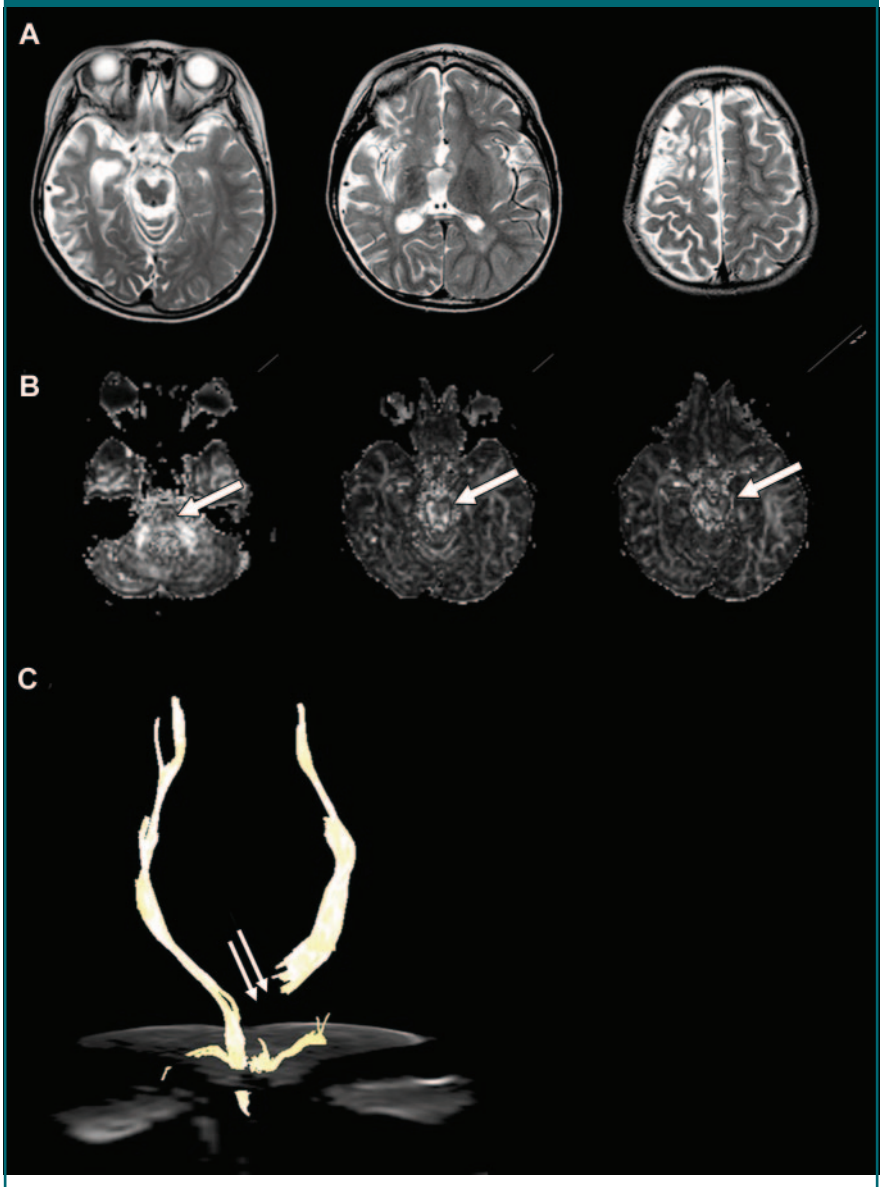

Figure 15: Images in 7-year-old boy involved in a vehicular accident 3 years before and suffering from intractable seizure. Electroencephalography demonstrated persistent discharge of epileptic wave in the right hemisphere. Functional right hemispherectomy was planned for treatment of the intractable seizure. However, patient demonstrated right-side hemiplegia instead of left-side dysfunction. *A,* Transverse T2-weighted (4000/100; matrix, 352 × 352; FOV, 230 × 230 mm; section thickness, 5 mm) images show cerebromalacia of right hemisphere and atrophy. Precentral gyrus is relatively spared. *B,* Fractional anisotropy maps show lack of high signal intensity of longitudinal pontine fiber tracts in the left-side cerebral peduncle, suggesting axonal injury (arrows). *C,* Fiber tractography with superimposed transverse *b*0 image shows cutting off of left corticospinal tract at the level of left cerebral peduncle due to axonal injury (arrows). Right corticospinal tract is intact although atrophy and cerebromalacia are demonstrated in the remainder of the brain. Callosotomy was performed instead of functional hemispherectomy on the basis of DT and fiber tractography findings, because right hemispherectomy would have resulted in quadriplegia (DT imaging: 32 directions; six-channel sensitivity encoding; sensitivity encoding factor of two; *b* value, 600 sec/mm^2; 6599–8280/70; matrix, 96 × 96; FOV, 220 × 220 mm; section thickness, 2.3 mm).

deficits after temporal lobe resection (215). Although preoperative tractography will probably be intended primarily for the delineation of white matter anatomy, it has also found use in mapping subservient gray matter such as primary motor cortex, particularly in patients unable to comply with the demands of BOLD functional MR imaging (216,217).

Conclusion

There is clearly a broad range of possible applications for DT imaging. However, the clinical status of DT imaging today is somewhat analogous to the status of DW imaging shortly after its introduction: Although the initial results appear promising, the prospective clinical trials that can fully establish its utility have yet to be completed. This will probably change in the future as an increasing number of long-term studies have begun to incorporate DT imaging into their protocols, while data regarding normal variability in DT imaging measures continue to accumulate (218). Nevertheless, the clinical use of DT imaging calls for careful understanding of acquisition and processing issues.

The full potential of DT imaging will probably not be realized until it is integrated with other modalities to obtain a richer characterization of white matter, in a manner analogous to the combination of perfusion and diffusion imaging data used to demonstrate an ischemic penumbra. Perhaps the most intriguing application is the integration of tractography with functional imaging. Activation maps are the natural complement of tractography; a temporal relationship between activated foci implies the existence of subservient fiber tracts, whereas anatomic connectivity between two regions of the brain suggests a functional relationship. The excellent correlation of BOLD functional MR data with tractography findings in motor and visual cortex may illustrate the future of structure-function investigations in the brain, ultimately to culminate in a comprehensive description of the "human connectome" (219).

References

1. Le Bihan D, Breton E, Lallemand D, Grenier P, Cabanis E, Laval-Jeantet M. MR imaging of intravoxel incoherent motions: application to diffusion and perfusion in neurologic disorders. Radiology 1986;161:401–407.
2. Moseley ME, Cohen Y, Kucharczyk J, et al. Diffusion-weighted MR imaging of anisotropic water diffusion in cat central nervous system. Radiology 1990;176:439–445.
3. Schellinger PD, Fiebach JB, Hacke W. Imaging-based decision making in thrombolytic therapy for ischemic stroke: present status. Stroke 2003;34:575–583.
4. Stejskal EO, Tanner JE. Spin diffusion measurements: spin echoes in the presence of a time-dependent field gradient. J Chem Phys 1965;42:288–292.
5. Moseley ME, Kucharczyk J, Asgari HS, Norman D. Anisotropy in diffusion-weighted MRI. Magn Reson Med 1991;19:321–326.
6. Song SK, Yoshino J, Le TQ, et al. Demyelination increases radial diffusivity in corpus callosum of mouse brain. Neuroimage 2005;26:132–140.
7. Henry RG, Oh J, Nelson SJ, Pelletier D. Directional diffusion in relapsing-remitting multiple sclerosis: a possible in vivo signature of Wallerian degeneration. J Magn Reson Imaging 2003;18:420–426.
8. Stanisz GJ, Midha R, Munro CA, Henkelman RM. MR properties of rat sciatic nerve following trauma. Magn Reson Med 2001;45:415–420.
9. Pierpaoli C, Barnett A, Pajevic S, et al. Water diffusion changes in Wallerian degeneration and their dependence on white matter architecture. Neuroimage 2001;13:1174–1185.
10. Beaulieu C, Does MD, Snyder RE, Allen PS. Changes in water diffusion due to Wallerian degeneration in peripheral nerve. Magn Reson Med 1996;36:627–631.
11. Song SK, Sun SW, Ju WK, Lin SJ, Cross AH, Neufeld AH. Diffusion tensor imaging detects and differentiates axon and myelin degeneration in mouse optic nerve after retinal ischemia. Neuroimage 2003;20:1714–1722.
12. Song SK, Sun SW, Ramsbottom MJ, Chang C, Russell J, Cross AH. Dysmyelination revealed through MRI as increased radial (but unchanged axial) diffusion of water. Neuroimage 2002;17:1429–1436.
13. Xing D, Papadakis NG, Huang CL, Lee VM, Carpenter TA, Hall LD. Optimised diffusion-weighting for measurement of apparent diffusion coefficient (ADC) in human brain. Magn Reson Imaging 1997;15:771–784.
14. Jones DK, Horsfield MA, Simmons A. Optimal strategies for measuring diffusion in anisotropic systems by magnetic resonance imaging. Magn Reson Med 1999;42:515–525.
15. Armitage PA, Bastin ME. Utilizing the diffusion-to-noise ratio to optimize magnetic resonance diffusion tensor acquisition strategies for improving measurements of diffusion anisotropy. Magn Reson Med 2001;45:1056–1065.
16. Kingsley PB, Monahan WG. Selection of the optimum b factor for diffusion-weighted magnetic resonance imaging assessment of ischemic stroke. Magn Reson Med 2004;51:996–1001.
17. Alexander DC, Barker GJ. Optimal imaging parameters for fiber-orientation estimation in diffusion MRI. Neuroimage 2005;27:357–367.
18. Hasan KM, Parker DL, Alexander AL. Comparison of gradient encoding schemes for diffusion-tensor MRI. J Magn Reson Imaging 2001;13:769–780.
19. Jones DK. The effect of gradient sampling schemes on measures derived from diffusion tensor MRI: a Monte Carlo study. Magn Reson Med 2004;51:807–815.
20. Turner R, Le Bihan DJ, Chesnick AS. Echo-planar imaging of diffusion and perfusion. Magn Reson Med 1991;19:247–253.
21. Andersson JL, Skare S. A model-based method for retrospective correction of geometric distortions in diffusion-weighted EPI. Neuroimage 2002;16:177–199.
22. Rohde GK, Barnett AS, Basser PJ, Marenco S, Pierpaoli C. Comprehensive approach for correction of motion and distortion in diffusion-weighted MRI. Magn Reson Med 2004;51:103–114.
23. Chang LC, Jones DK, Pierpaoli C. RESTORE: robust estimation of tensors by outlier rejection. Magn Reson Med 2005;53:1088–1095.
24. Rohde GK, Barnett AS, Basser PJ, Pierpaoli C. Estimating intensity variance due to noise in registered images: applications to diffusion tensor MRI. Neuroimage 2005;26:673–684.
25. Haselgrove JC, Moore JR. Correction for distortion of echo-planar images used to calculate the apparent diffusion coefficient. Magn Reson Med 1996;36:960–964.
26. Alexander AL, Tsuruda JS, Parker DL.

Elimination of eddy current artifacts in diffusion-weighted echo-planar images: the use of bipolar gradients. Magn Reson Med 1997;38:1016–1021.

27. Jones DK, Basser PJ. "Squashing peanuts and smashing pumpkins": how noise distorts diffusion-weighted MR data. Magn Reson Med 2004;52:979–993.
28. Skare S, Andersson JL. On the effects of gating in diffusion imaging of the brain using single shot EPI. Magn Reson Imaging 2001;19:1125–1128.
29. Bhagat YA, Beaulieu C. Diffusion anisotropy in subcortical white matter and cortical gray matter: changes with aging and the role of CSF-suppression. J Magn Reson Imaging 2004;20:216–227.
30. Papadakis NG, Martin KM, Mustafa MH, et al. Study of the effect of CSF suppression on white matter diffusion anisotropy mapping of healthy human brain. Magn Reson Med 2002;48:394–398.
31. Falconer JC, Narayana PA. Cerebrospinal fluid-suppressed high-resolution diffusion imaging of human brain. Magn Reson Med 1997;37:119–123.
32. Hirsch JG, Bock M, Essig M, Schad LR. Comparison of diffusion anisotropy measurements in combination with the flair-technique. Magn Reson Imaging 1999;17:705–716.
33. Kwong KK, McKinstry RC, Chien D, Crawley AP, Pearlman JD, Rosen BR. CSF-suppressed quantitative single-shot diffusion imaging. Magn Reson Med 1991;21:157–163.
34. Rieseberg S, Merboldt KD, Kuntzel M, Frahm J. Diffusion tensor imaging using partial Fourier STEAM MRI with projection onto convex subsets reconstruction. Magn Reson Med 2005;54:486–490.
35. Bammer R. Basic principles of diffusion-weighted imaging. Eur J Radiol 2003;45:169–184.
36. Gudbjartsson H, Maier SE, Mulkern RV, Morocz IA, Patz S, Jolesz FA. Line scan diffusion imaging. Magn Reson Med 1996;36:509–519.
37. Finsterbusch J, Frahm J. Diffusion tensor mapping of the human brain using single-shot line scan imaging. J Magn Reson Imaging 2000;12:388–394.
38. Forbes KP, Pipe JG, Karis JP, Heiserman JE. Improved image quality and detection of acute cerebral infarction with PROPELLER diffusion-weighted MR imaging. Radiology 2002;225:551–555.
39. Pipe JG, Farthing VG, Forbes KP. Multi-shot diffusion-weighted FSE using PROPELLER MRI. Magn Reson Med 2002;47:42–52.
40. Pipe JG, Zwart N. Turboprop: improved PROPELLER imaging. Magn Reson Med 2006;55:380–385.
41. Liu C, Bammer R, Kim DH, Moseley ME. Self-navigated interleaved spiral (SNAILS): application to high-resolution diffusion tensor imaging. Magn Reson Med 2004;52:1388–1396.
42. Liu C, Moseley ME, Bammer R. Simultaneous phase correction and SENSE reconstruction for navigated multi-shot DWI with non-cartesian k-space sampling. Magn Reson Med 2005;54:1412–1422.
43. Bammer R, Auer M, Keeling SL, et al. Diffusion tensor imaging using single-shot SENSE-EPI. Magn Reson Med 2002;48:128–136.
44. Bammer R, Keeling SL, Augustin M, et al. Improved diffusion-weighted single-shot echo-planar imaging (EPI) in stroke using sensitivity encoding (SENSE). Magn Reson Med 2001;46:548–554.
45. Basser PJ, Mattiello J, Le Bihan DJ. Estimation of the effective self-diffusion tensor from the NMR spin echo. J Magn Reson B 1994;103:247–254.
46. Lazar M, Alexander AL. An error analysis of white matter tractography methods: synthetic diffusion tensor field simulations. Neuroimage 2003;20:1140–1153.
47. Pierpaoli C, Jezzard P, Basser PJ, Barnett A, Di CG. Diffusion tensor MR imaging of the human brain. Radiology 1996;201:637–648.
48. Okada T, Miki Y, Fushimi Y, et al. Diffusion-tensor fiber tractography: intraindividual comparison of 3.0-T and 1.5-T MR imaging. Radiology 2006;238:668–678.
49. Tuch DS, Reese TG, Wiegell MR, Makris N, Belliveau JW, Wedeen VJ. High angular resolution diffusion imaging reveals intravoxel white matter fiber heterogeneity. Magn Reson Med 2002;48:577–582.
50. Tuch DS, Reese TG, Wiegell MR, Wedeen VJ. Diffusion MRI of complex neural architecture. Neuron 2003;40:885–895.
51. Ozarslan E, Mareci TH. Generalized diffusion tensor imaging and analytical relationships between diffusion tensor imaging and high angular resolution diffusion imaging. Magn Reson Med 2003;50:955–965.
52. Cory DG, Garroway AN. Measurement of translational displacement probabilities by NMR: an indicator of compartmentation. Magn Reson Med 1990;14:435–444.
53. Callaghan PT, Codd SL, Seymour JD. Spatial coherence phenomena arising from translational spin motion in gradient spin echo experiments. SO Concepts Magn Reson 1999;11:181–202.
54. Hagmann P, Jonasson L, Maeder P, Thiran JP, van Wedeen J, Meuli R. Understanding diffusion MR imaging techniques: from scalar diffusion-weighted imaging to diffusion tensor imaging and beyond. RadioGraphics 2006;26(suppl 1):S205–S223.
55. Basser PJ. Relationships between diffusion tensor and q-space MRI. Magn Reson Med 2002;47:392–397.
56. Frank LR. Characterization of anisotropy in high angular resolution diffusion-weighted MRI. Magn Reson Med 2002;47:1083–1099.
57. Alexander DC. Multiple-fiber reconstruction algorithms for diffusion MRI. Ann N Y Acad Sci 2005;1064:113–133.
58. Tournier JD, Calamante F, Gadian DG, Connelly A. Direct estimation of the fiber orientation density function from diffusion-weighted MRI data using spherical deconvolution. Neuroimage 2004;23:1176–1185.
59. Lin CP, Wedeen VJ, Chen JH, Yao C, Tseng WY. Validation of diffusion spectrum magnetic resonance imaging with manganese-enhanced rat optic tracts and ex vivo phantoms. Neuroimage 2003;19:482–495.
60. Tuch DS. Q-ball imaging. Magn Reson Med 2004;52:1358–1372.
61. Campbell JS, Siddiqi K, Rymar VV, Sadikot AF, Pike GB. Flow-based fiber tracking with diffusion tensor and q-ball data: validation and comparison to principal diffusion direction techniques. Neuroimage 2005;27:725–736.
62. Perrin M, Poupon C, Rieul B, et al. Validation of q-ball imaging with a diffusion fibre-crossing phantom on a clinical scanner. Philos Trans R Soc Lond B Biol Sci 2005;360:881–891.
63. Mori S, Crain BJ, Chacko VP, van Zijl PC. Three-dimensional tracking of axonal projections in the brain by magnetic resonance imaging. Ann Neurol 1999;45:265–269.
64. Masutani Y, Aoki S, Abe O, Hayashi N, Otomo K. MR diffusion tensor imaging: recent advance and new techniques for diffusion tensor visualization. Eur J Radiol 2003;46:53–66.
65. Westin CF, Maier SE, Mamata H, Nabavi A, Jolesz FA, Kikinis R. Processing and visualization for diffusion tensor MRI. Med Image Anal 2002;6:93–108.
66. Lazar M, Weinstein DM, Tsuruda JS, et al.

White matter tractography using diffusion tensor deflection. Hum Brain Mapp 2003; 18:306–321.

67. Conturo TE, Lori NF, Cull TS, et al. Tracking neuronal fiber pathways in the living human brain. Proc Natl Acad Sci U S A 1999;96:10422–10427.

68. Basser PJ, Pajevic S, Pierpaoli C, Duda J, Aldroubi A. In vivo fiber tractography using DT-MRI data. Magn Reson Med 2000;44: 625–632.

69. Behrens TE, Johansen-Berg H, Woolrich MW, et al. Non-invasive mapping of connections between human thalamus and cortex using diffusion imaging. Nat Neurosci 2003;6:750–757.

70. Parker GJ, Haroon HA, Wheeler-Kingshott CA. A framework for a streamline-based probabilistic index of connectivity (PICo) using a structural interpretation of MRI diffusion measurements. J Magn Reson Imaging 2003;18:242–254.

71. Parker GJ, Stephan KE, Barker GJ, et al. Initial demonstration of in vivo tracing of axonal projections in the macaque brain and comparison with the human brain using diffusion tensor imaging and fast marching tractography. Neuroimage 2002;15: 797–809.

72. Jackowski M, Kao CY, Qiu M, Constable RT, Staib LH. White matter tractography by anisotropic wavefront evolution and diffusion tensor imaging. Med Image Anal 2005;9:427–440.

73. Staempfli P, Jaermann T, Crelier GR, Kollias S, Valavanis A, Boesiger P. Resolving fiber crossing using advanced fast marching tractography based on diffusion tensor imaging. Neuroimage 2006;30:110–120.

74. Cercignani M, Bammer R, Sormani MP, Fazekas F, Filippi M. Inter-sequence and inter-imaging unit variability of diffusion tensor MR imaging histogram-derived metrics of the brain in healthy volunteers. AJNR Am J Neuroradiol 2003;24:638–643.

75. Wakana S, Jiang H, Nagae-Poetscher LM, van Zijl PC, Mori S. Fiber tract-based atlas of human white matter anatomy. Radiology 2004;230:77–87.

76. Stieltjes B, Kaufmann WE, van Zijl PC, et al. Diffusion tensor imaging and axonal tracking in the human brainstem. Neuroimage 2001;14:723–735.

77. Ciccarelli O, Parker GJ, Toosy AT, et al. From diffusion tractography to quantitative white matter tract measures: a reproducibility study. Neuroimage 2003;18:348–359.

78. Wu YC, Field AS, Chung MK, Badie B, Alexander AL. Quantitative analysis of diffusion tensor orientation: theoretical framework. Magn Reson Med 2004;52: 1146–1155.

79. Fletcher P, Joshi S. Principal geodesic analysis on symmetric spaces: statistics of diffusion tensors. Proceedings of the ECCV 2004 Workshop on Computer Vision Approaches to Medical Image Analysis: lecture notes in computer science. Vol 3117. Prague, Czech Republic; Springer-Verlag, 2004: 87–98.

80. Jones DK. Determining and visualizing uncertainty in estimates of fiber orientation from diffusion tensor MRI. Magn Reson Med 2003;49:7–12.

81. Lazar M, Alexander AL. Bootstrap white matter tractography (BOOT-TRAC). Neuroimage 2005;24:524–532.

82. Jones DK, Pierpaoli C. Confidence mapping in diffusion tensor magnetic resonance imaging tractography using a bootstrap approach. Magn Reson Med 2005;53:1143–1149.

83. Heim S, Hahn K, Samann PG, Fahrmeir L, Auer DP. Assessing DTI data quality using bootstrap analysis. Magn Reson Med 2004; 52:582–589.

84. Steens SC, Admiraal-Behloul F, Schaap JA, et al. Reproducibility of brain ADC histograms. Eur Radiol 2004;14:425–430.

85. Mascalchi M, Tessa C, Moretti M, et al. Whole brain apparent diffusion coefficient histogram: a new tool for evaluation of leukoaraiosis. J Magn Reson Imaging 2002;15: 144–148.

86. Nyul LG, Udupa JK. On standardizing the MR image intensity scale. Magn Reson Med 1999;42:1072–1081.

87. Anbeek P, Vincken KL, van Osch MJ, Bisschops RH, van der Grond J. Probabilistic segmentation of white matter lesions in MR imaging. Neuroimage 2004;21:1037–1044.

88. Lin CY, Sun SW, Hong CY, Chang C. Unsupervised identification of white matter tracts in a mouse brain using a directional correlation-based region growing (DCRG) algorithm. Neuroimage 2005;28:380–388.

89. Bilgili Y, Unal B. Effect of region of interest on interobserver variance in apparent diffusion coefficient measures. AJNR Am J Neuroradiol 2004;25:108–111.

90. Tzourio-Mazoyer N, Landeau B, Papathanassiou D, et al. Automated anatomical labeling of activations in SPM using a macroscopic anatomical parcellation of the MNI MRI single-subject brain. Neuroimage 2002;15: 273–289.

91. Alexander DC, Pierpaoli C, Basser PJ, Gee JC. Spatial transformations of diffusion tensor magnetic resonance images. IEEE Trans Med Imaging 2001;20:1131–1139.

92. Park HJ, Kubicki M, Shenton ME, et al. Spatial normalization of diffusion tensor MRI using multiple channels. Neuroimage 2003;20:1995–2009.

93. Xu D, Mori S, Shen D, van Zijl PC, Davatzikos C. Spatial normalization of diffusion tensor fields. Magn Reson Med 2003;50:175–182.

94. Turner R, Howseman A, Rees GE, Josephs O, Friston K. Functional magnetic resonance imaging of the human brain: data acquisition and analysis. Exp Brain Res 1998;123:5–12.

95. Ciccarelli O, Toosy AT, Parker GJ, et al. Diffusion tractography based group mapping of major white-matter pathways in the human brain. Neuroimage 2003;19:1545–1555.

96. Jones DK, Symms MR, Cercignani M, Howard RJ. The effect of filter size on VBM analyses of DT-MRI data. Neuroimage 2005;26:546–554.

97. Davatzikos C. Why voxel-based morphometric analysis should be used with great caution when characterizing group differences. Neuroimage 2004;23:17–20.

98. Huang H, Zhang J, Jiang H, et al. DTI tractography based parcellation of white matter: application to the mid-sagittal morphology of corpus callosum. Neuroimage 2005;26:195–205.

99. Partridge SC, Mukherjee P, Berman JI, et al. Tractography-based quantitation of diffusion tensor imaging parameters in white matter tracts of preterm newborns. J Magn Reson Imaging 2005;22:467–474.

100. Fillard P, Gilmore JH, Lin W, Piven J, Gerig G. Quantitative analysis of white matter fiber properties along geodesic paths. Proceedings of the 6th International Conference on Medical Image Computing and Computer-Assisted Intervention: MICCAI 2003—lecture notes in computer science. Vol 2879. Montreal, Canada: 2003; 16–23.

101. Jones DK, Travis AR, Eden G, Pierpaoli C, Basser PJ. PASTA: pointwise assessment of streamline tractography attributes. Magn Reson Med 2005;53:1462–1467.

102. Gong G, Jiang T, Zhu C, et al. Asymmetry analysis of cingulum based on scale-invariant parameterization by diffusion tensor imaging. Hum Brain Mapp 2005;24:92–98.

103. Johansen-Berg H, Behrens TE, Robson

MD, et al. Changes in connectivity profiles define functionally distinct regions in human medial frontal cortex. Proc Natl Acad Sci U S A 2004;101:13335–13340.

104. Schmithorst VJ, Wilke M, Dardzinski BJ, Holland SK. Cognitive functions correlate with white matter architecture in a normal pediatric population: a diffusion tensor MRI study. Hum Brain Mapp 2005;26:139–147.

105. Lazar M, Field A, Lee J, Alexander AL. Lateral asymmetry of the superior longitudinal fasciculus: a white matter tractography study (abstr). In: Proceedings of the 12th Meeting of the International Society for Magnetic Resonance in Medicine. Berkeley, Calif: International Society for Magnetic Resonance in Medicine, 2004; 1290.

106. Beaulieu C, Plewes C, Paulson LA, et al. Imaging brain connectivity in children with diverse reading ability. Neuroimage 2005; 25:1266–1271.

107. Parker GJ, Luzzi S, Alexander DC, Wheeler-Kingshott CA, Ciccarelli O, Lambon Ralph MA. Lateralization of ventral and dorsal auditory-language pathways in the human brain. Neuroimage 2005;24:656–666.

108. Nucifora PG, Verma R, Melhem ER, Gur RE, Gur RC. Leftward asymmetry in relative fiber density of the arcuate fasciculus. Neuroreport 2005;16:791–794.

109. Klingberg T, Hedehus M, Temple E, et al. Microstructure of temporo-parietal white matter as a basis for reading ability: evidence from diffusion tensor magnetic resonance imaging. Neuron 2000;25:493–500.

110. Deutsch GK, Dougherty RF, Bammer R, Siok WT, Gabrieli JD, Wandell B. Children's reading performance is correlated with white matter structure measured by diffusion tensor imaging. Cortex 2005;41: 354–363.

111. Tuch DS, Salat DH, Wisco JJ, Zaleta AK, Hevelone ND, Rosas HD. Choice reaction time performance correlates with diffusion anisotropy in white matter pathways supporting visuospatial attention. Proc Natl Acad Sci U S A 2005;102:12212–12217.

112. Shimony JS, Burton H, Epstein AA, McLaren DG, Sun SW, Snyder AZ. Diffusion tensor imaging reveals white matter reorganization in early blind humans. Cereb Cortex 2006;16:1653–1661.

113. Dougherty RF, Ben-Shachar M, Bammer R, Brewer AA, Wandell BA. Functional organization of human occipital-callosal fiber tracts. Proc Natl Acad Sci U S A 2005;102: 7350–7355.

114. Dougherty RF, Ben-Shachar M, Deutsch G, Potanina P, Bammer R, Wandell BA. Occipital-callosal pathways in children: validation and atlas development. Ann N Y Acad Sci 2005;1064:98–112.

115. Johansen-Berg H, Behrens TE, Sillery E, et al. Functional-anatomical validation and individual variation of diffusion tractography-based segmentation of the human thalamus. Cereb Cortex 2005;15:31–39.

116. Toosy AT, Ciccarelli O, Parker GJ, Wheeler-Kingshott CA, Miller DH, Thompson AJ. Characterizing function-structure relationships in the human visual system with functional MRI and diffusion tensor imaging. Neuroimage 2004;21:1452–1463.

117. Deipolyi AR, Mukherjee P, Gill K, et al. Comparing microstructural and macrostructural development of the cerebral cortex in premature newborns: diffusion tensor imaging versus cortical gyration. Neuroimage 2005;27:579–586.

118. Hermoye L, Saint-Martin C, Cosnard G, et al. Pediatric diffusion tensor imaging: normal database and observation of the white matter maturation in early childhood. Neuroimage 2006;29:493–504.

119. Berman JI, Mukherjee P, Partridge SC, et al. Quantitative diffusion tensor MRI fiber tractography of sensorimotor white matter development in premature infants. Neuroimage 2005;27:862–871.

120. Partridge SC, Mukherjee P, Henry RG, et al. Diffusion tensor imaging: serial quantitation of white matter tract maturity in premature newborns. Neuroimage 2004; 22:1302–1314.

121. Maas LC, Mukherjee P, Carballido-Gamio J, et al. Early laminar organization of the human cerebrum demonstrated with diffusion tensor imaging in extremely premature infants. Neuroimage 2004;22:1134–1140.

122. Huppi PS, Maier SE, Peled S, et al. Microstructural development of human newborn cerebral white matter assessed in vivo by diffusion tensor magnetic resonance imaging. Pediatr Res 1998;44:584–590.

123. Neil JJ, Shiran SI, McKinstry RC, et al. Normal brain in human newborns: apparent diffusion coefficient and diffusion anisotropy measured by using diffusion tensor MR imaging. Radiology 1998;209:57–66.

124. McKinstry RC, Mathur A, Miller JH, et al. Radial organization of developing preterm human cerebral cortex revealed by non-invasive water diffusion anisotropy MRI. Cereb Cortex 2002;12:1237–1243.

125. Mukherjee P, Miller JH, Shimony JS, et al. Diffusion-tensor MR imaging of gray and white matter development during normal human brain maturation. AJNR Am J Neuroradiol 2002;23:1445–1456.

126. Mori S, Itoh R, Zhang J, et al. Diffusion tensor imaging of the developing mouse brain. Magn Reson Med 2001;46:18–23.

127. Verma R, Mori S, Shen D, Yarowsky P, Zhang J, Davatzikos C. Spatiotemporal maturation patterns of murine brain quantified by diffusion tensor MRI and deformation-based morphometry. Proc Natl Acad Sci U S A 2005;102:6978–6983.

128. Eriksson SH, Rugg-Gunn FJ, Symms MR, Barker GJ, Duncan JS. Diffusion tensor imaging in patients with epilepsy and malformations of cortical development. Brain 2001;124:617–626.

129. Eriksson SH, Symms MR, Rugg-Gunn FJ, et al. Exploring white matter tracts in band heterotopia using diffusion tractography. Ann Neurol 2002;52:327–334.

130. Rollins N, Reyes T, Chia J. Diffusion tensor imaging in lissencephaly. AJNR Am J Neuroradiol 2005;26:1583–1586.

131. Hoon AH Jr, Lawrie WT Jr, Melhem ER, et al. Diffusion tensor imaging of periventricular leukomalacia shows affected sensory cortex white matter pathways. Neurology 2002;59:752–756.

132. Thomas B, Eyssen M, Peeters R, et al. Quantitative diffusion tensor imaging in cerebral palsy due to periventricular white matter injury. Brain 2005;128:2562–2577.

133. Albayram S, Melhem ER, Mori S, Zinreich SJ, Barkovich AJ, Kinsman SL. Holoprosencephaly in children: diffusion tensor MR imaging of white matter tracts of the brainstem—initial experience. Radiology 2002;223:645–651.

134. Salat DH, Tuch DS, Greve DN, et al. Age-related alterations in white matter microstructure measured by diffusion tensor imaging. Neurobiol Aging 2005;26:1215–1227.

135. Rovaris M, Iannucci G, Cercignani M, et al. Age-related changes in conventional, magnetization transfer, and diffusion-tensor MR imaging findings: study with whole-brain tissue histogram analysis. Radiology 2003;227:731–738.

136. Pfefferbaum A, Sullivan EV, Hedehus M, Lim KO, Adalsteinsson E, Moseley M. Age-related decline in brain white matter anisotropy measured with spatially corrected echo-planar diffusion tensor imaging. Magn Reson Med 2000;44:259–268.

137. Sullivan EV, Adalsteinsson E, Hedehus M, et al. Equivalent disruption of regional white matter microstructure in ageing

healthy men and women. Neuroreport 2001;12:99–104.

138. Yoshikawa K, Nakata Y, Yamada K, Nakagawa M. Early pathological changes in the parkinsonian brain demonstrated by diffusion tensor MRI. J Neurol Neurosurg Psychiatry 2004;75:481–484.

139. Bozzali M, Falini A, Franceschi M, et al. White matter damage in Alzheimer's disease assessed in vivo using diffusion tensor magnetic resonance imaging. J Neurol Neurosurg Psychiatry 2002;72:742–746.

140. Rose SE, Chen F, Chalk JB, et al. Loss of connectivity in Alzheimer's disease: an evaluation of white matter tract integrity with colour coded MR diffusion tensor imaging. J Neurol Neurosurg Psychiatry 2000; 69:528–530.

141. Bozzali M, Falini A, Cercignani M, et al. Brain tissue damage in dementia with Lewy bodies: an in vivo diffusion tensor MRI study. Brain 2005;128:1595–1604.

142. Nierenberg J, Pomara N, Hoptman MJ, Sidtis JJ, Ardekani BA, Lim KO. Abnormal white matter integrity in healthy apolipoprotein E epsilon4 carriers. Neuroreport 2005;16:1369–1372.

143. Reading SA, Yassa MA, Bakker A, et al. Regional white matter change in pre-symptomatic Huntington's disease: a diffusion tensor imaging study. Psychiatry Res 2005; 140:55–62.

144. Cosottini M, Giannelli M, Siciliano G, et al. Diffusion-tensor MR imaging of corticospinal tract in amyotrophic lateral sclerosis and progressive muscular atrophy. Radiology 2005;237:258–264.

145. Wang S, Melhem ER. Amyotrophic lateral sclerosis and primary lateral sclerosis: the role of diffusion tensor imaging and other advanced MR-based techniques as objective upper motor neuron markers. Ann N Y Acad Sci 2005;1064:61–77.

146. Hong YH, Lee KW, Sung JJ, Chang KH, Song IC. Diffusion tensor MRI as a diagnostic tool of upper motor neuron involvement in amyotrophic lateral sclerosis. J Neurol Sci 2004;227:73–78.

147. Toosy AT, Werring DJ, Orrell RW, et al. Diffusion tensor imaging detects corticospinal tract involvement at multiple levels in amyotrophic lateral sclerosis. J Neurol Neurosurg Psychiatry 2003;74:1250–1257.

148. Yin H, Lim CC, Ma L, et al. Combined MR spectroscopic imaging and diffusion tensor MRI visualizes corticospinal tract degeneration in amyotrophic lateral sclerosis. J Neurol 2004;251:1249–1254.

149. Karlsborg M, Rosenbaum S, Wiegell M, et al. Corticospinal tract degeneration and possible pathogenesis in ALS evaluated by MR diffusion tensor imaging. Amyotroph Lateral Scler Other Motor Neuron Disord 2004;5:136–140.

150. Graham JM, Papadakis N, Evans J, et al. Diffusion tensor imaging for the assessment of upper motor neuron integrity in ALS. Neurology 2004;63:2111–2119.

151. Ellis CM, Simmons A, Jones DK, et al. Diffusion tensor MRI assesses corticospinal tract damage in ALS. Neurology 1999;53: 1051–1058.

152. Jacob S, Finsterbusch J, Weishaupt JH, Khorram-Sefat D, Frahm J, Ehrenreich H. Diffusion tensor imaging for long-term follow-up of corticospinal tract degeneration in amyotrophic lateral sclerosis. Neuroradiology 2003;45:598–600.

153. Abe O, Yamada H, Masutani Y, et al. Amyotrophic lateral sclerosis: diffusion tensor tractography and voxel-based analysis. NMR Biomed 2004;17:411–416.

154. Sach M, Winkler G, Glauche V, et al. Diffusion tensor MRI of early upper motor neuron involvement in amyotrophic lateral sclerosis. Brain 2004;127:340–350.

155. Price G, Bagary MS, Cercignani M, Altmann DR, Ron MA. The corpus callosum in first episode schizophrenia: a diffusion tensor imaging study. J Neurol Neurosurg Psychiatry 2005;76:585–587.

156. Kubicki M, Westin CF, Nestor PG, et al. Cingulate fasciculus integrity disruption in schizophrenia: a magnetic resonance diffusion tensor imaging study. Biol Psychiatry 2003;54:1171–1180.

157. Lim KO, Hedehus MP, Moseley M, de Crespigny A, Sullivan EV, Pfefferbaum AM. Compromised white matter tract integrity in schizophrenia inferred from diffusion tensor imaging. Arch Gen Psychiatry 1999; 56:367–374.

158. Kubicki M, Park H, Westin CF, et al. DTI and MTR abnormalities in schizophrenia: analysis of white matter integrity. Neuroimage 2005;26:1109–1118.

159. Nestor PG, Kubicki M, Gurrera RJ, et al. Neuropsychological correlates of diffusion tensor imaging in schizophrenia. Neuropsychology 2004;18:629–637.

160. Hubl D, Koenig T, Strik W, et al. Pathways that make voices: white matter changes in auditory hallucinations. Arch Gen Psychiatry 2004;61:658–668.

161. Kanaan RA, Kim JS, Kaufmann WE, Pearlson GD, Barker GJ, McGuire PK. Diffusion tensor imaging in schizophrenia. Biol Psychiatry 2005;58:921–929.

162. Szeszko PR, Ardekani BA, Ashtari M, et al. White matter abnormalities in first-episode schizophrenia or schizoaffective disorder: a diffusion tensor imaging study. Am J Psychiatry 2005;162:602–605.

163. Kalus P, Slotboom J, Gallinat J, et al. New evidence for involvement of the entorhinal region in schizophrenia: a combined MRI volumetric and DTI study. Neuroimage 2005;24:1122–1129.

164. Jones DK, Catani M, Pierpaoli C, et al. A diffusion tensor magnetic resonance imaging study of frontal cortex connections in very-late-onset schizophrenia-like psychosis. Am J Geriatr Psychiatry 2005;13:1092–1099.

165. Jones DK, Catani M, Pierpaoli C, et al. Age effects on diffusion tensor magnetic resonance imaging tractography measures of frontal cortex connections in schizophrenia. Hum Brain Mapp 2006;27:230–238.

166. Kanaan RA, Shergill SS, Barker GJ, et al. Tract-specific anisotropy measurements in diffusion tensor imaging. Psychiatry Res 2006;146:73–82.

167. Adler CM, Holland SK, Schmithorst V, et al. Abnormal frontal white matter tracts in bipolar disorder: a diffusion tensor imaging study. Bipolar Disord 2004;6:197–203.

168. Li TQ, Mathews VP, Wang Y, Dunn D, Kronenberger W. Adolescents with disruptive behavior disorder investigated using an optimized MR diffusion tensor imaging protocol. Ann N Y Acad Sci 2005;1064:184–192.

169. Taylor WD, MacFall JR, Payne ME, et al. Late-life depression and microstructural abnormalities in dorsolateral prefrontal cortex white matter. Am J Psychiatry 2004; 161:1293–1296.

170. Barnea-Goraly N, Kwon H, Menon V, Eliez S, Lotspeich L, Reiss AL. White matter structure in autism: preliminary evidence from diffusion tensor imaging. Biol Psychiatry 2004;55:323–326.

171. Szeszko PR, Ardekani BA, Ashtari M, et al. White matter abnormalities in obsessive-compulsive disorder: a diffusion tensor imaging study. Arch Gen Psychiatry 2005;62: 782–790.

172. Ashtari M, Kumra S, Bhaskar SL, et al. Attention-deficit/hyperactivity disorder: a preliminary diffusion tensor imaging study. Biol Psychiatry 2005;57:448–455.

173. Pfefferbaum A, Sullivan EV, Hedehus M, Adalsteinsson E, Lim KO, Moseley M. In vivo detection and functional correlates of white matter microstructural disruption

in chronic alcoholism. Alcohol Clin Exp Res 2000;24:1214–1221.

174. Moeller FG, Hasan KM, Steinberg JL, et al. Reduced anterior corpus callosum white matter integrity is related to increased impulsivity and reduced discriminability in cocaine-dependent subjects: diffusion tensor imaging. Neuropsychopharmacology 2005; 30:610–617.

175. Filippi M, Cercignani M, Inglese M, Horsfield MA, Comi G. Diffusion tensor magnetic resonance imaging in multiple sclerosis. Neurology 2001;56:304–311.

176. Castriota-Scanderbeg A, Fasano F, Hagberg G, Nocentini U, Filippi M, Caltagirone C. Coefficient D(av) is more sensitive than fractional anisotropy in monitoring progression of irreversible tissue damage in focal nonactive multiple sclerosis lesions. AJNR Am J Neuroradiol 2003;24:663–670.

177. Roychowdhury S, Maldjian JA, Grossman RI. Multiple sclerosis: comparison of trace apparent diffusion coefficients with MR enhancement pattern of lesions. AJNR Am J Neuroradiol 2000;21:869–874.

178. Tievsky AL, Ptak T, Farkas J. Investigation of apparent diffusion coefficient and diffusion tensor anisotrophy in acute and chronic multiple sclerosis lesions. AJNR Am J Neuroradiol 1999;20:1491–1499.

179. Bammer R, Augustin M, Strasser-Fuchs S, et al. Magnetic resonance diffusion tensor imaging for characterizing diffuse and focal white matter abnormalities in multiple sclerosis. Magn Reson Med 2000;44:583–591.

180. Droogan AG, Clark CA, Werring DJ, Barker GJ, McDonald WI, Miller DH. Comparison of multiple sclerosis clinical subgroups using navigated spin echo diffusion-weighted imaging. Magn Reson Imaging 1999;17:653–661.

181. Werring DJ, Clark CA, Barker GJ, Thompson AJ, Miller DH. Diffusion tensor imaging of lesions and normal-appearing white matter in multiple sclerosis. Neurology 1999;52: 1626–1632.

182. Rovaris M, Gallo A, Valsasina P, et al. Short-term accrual of gray matter pathology in patients with progressive multiple sclerosis: an in vivo study using diffusion tensor MRI. Neuroimage 2005;24:1139–1146.

183. Vrenken H, Pouwels PJ, Geurts JJ, et al. Altered diffusion tensor in multiple sclerosis normal-appearing brain tissue: cortical diffusion changes seem related to clinical deterioration. J Magn Reson Imaging 2006; 23:628–636.

184. Bozzali M, Cercignani M, Sormani MP, Comi G, Filippi M. Quantification of brain gray matter damage in different MS phenotypes by use of diffusion tensor MR imaging. AJNR Am J Neuroradiol 2002;23:985–988.

185. Pagani E, Filippi M, Rocca MA, Horsfield MA. A method for obtaining tract-specific diffusion tensor MRI measurements in the presence of disease: application to patients with clinically isolated syndromes suggestive of multiple sclerosis. Neuroimage 2005;26:258–265.

186. Lee JS, Han MK, Kim SH, Kwon OK, Kim JH. Fiber tracking by diffusion tensor imaging in corticospinal tract stroke: topographical correlation with clinical symptoms. Neuroimage 2005;26:771–776.

187. Werring DJ, Toosy AT, Clark CA, et al. Diffusion tensor imaging can detect and quantify corticospinal tract degeneration after stroke. J Neurol Neurosurg Psychiatry 2000;69:269–272.

188. Konishi J, Yamada K, Kizu O, et al. MR tractography for the evaluation of functional recovery from lenticulostriate infarcts. Neurology 2005;64:108–113.

189. Kunimatsu A, Aoki S, Masutani Y, Abe O, Mori H, Ohtomo K. Three-dimensional white matter tractography by diffusion tensor imaging in ischaemic stroke involving the corticospinal tract. Neuroradiology 2003; 45:532–535.

190. Yamada K, Mori S, Nakamura H, et al. Fiber-tracking method reveals sensorimotor pathway involvement in stroke patients. Stroke 2003;34:E159–E162.

191. Yamada K, Ito H, Nakamura H, et al. Stroke patients' evolving symptoms assessed by tractography. J Magn Reson Imaging 2004;20:923–929.

192. Heller SL, Heier LA, Watts R, et al. Evidence of cerebral reorganization following perinatal stroke demonstrated with fMRI and DTI tractography. Clin Imaging 2005; 29:283–287.

193. Chabriat H, Pappata S, Poupon C, et al. Clinical severity in CADASIL related to ultrastructural damage in white matter: in vivo study with diffusion tensor MRI. Stroke 1999;30:2637–2643.

194. O'Sullivan M, Barrick TR, Morris RG, Clark CA, Markus HS. Damage within a network of white matter regions underlies executive dysfunction in CADASIL. Neurology 2005; 65:1584–1590.

195. Lu S, Ahn D, Johnson G, Law M, Zagzag D, Grossman RI. Diffusion-tensor MR imaging of intracranial neoplasia and associated peritumoral edema: introduction of the tumor infiltration index. Radiology 2004;232: 221–228.

196. Lu S, Ahn D, Johnson G, Cha S. Peritumoral diffusion tensor imaging of high-grade gliomas and metastatic brain tumors. AJNR Am J Neuroradiol 2003;24:937–941.

197. Tropine A, Vucurevic G, Delani P, et al. Contribution of diffusion tensor imaging to delineation of gliomas and glioblastomas. J Magn Reson Imaging 2004;20:905–912.

198. Provenzale JM, McGraw P, Mhatre P, Guo AC, Delong D. Peritumoral brain regions in gliomas and meningiomas: investigation with isotropic diffusion-weighted MR imaging and diffusion-tensor MR imaging. Radiology 2004;232:451–460.

199. Le Bihan D, Douek P, Argyropoulou M, Turner R, Patronas N, Fulham M. Diffusion and perfusion magnetic resonance imaging in brain tumors. Top Magn Reson Imaging 1993;5:25–31.

200. Tien RD, Felsberg GJ, Friedman H, Brown M, Macfall J. MR imaging of high-grade cerebral gliomas: value of diffusion-weighted echoplanar pulse sequences. AJR Am J Roentgenol 1994;162:671–677.

201. Hamstra DA, Chenevert TL, Moffat BA, et al. Evaluation of the functional diffusion map as an early biomarker of time-to-progression and overall survival in high-grade glioma. Proc Natl Acad Sci U S A 2005;102: 16759–16764.

202. Moffat BA, Chenevert TL, Lawrence TS, et al. Functional diffusion map: a noninvasive MRI biomarker for early stratification of clinical brain tumor response. Proc Natl Acad Sci U S A 2005;102:5524–5529.

203. Clark CA, Barrick TR, Murphy MM, Bell BA. White matter fiber tracking in patients with space-occupying lesions of the brain: a new technique for neurosurgical planning? Neuroimage 2003;20:1601–1608.

204. Field AS, Alexander AL, Wu YC, Hasan KM, Witwer B, Badie B. Diffusion tensor eigenvector directional color imaging patterns in the evaluation of cerebral white matter tracts altered by tumor. J Magn Reson Imaging 2004;20:555–562.

205. Mori S, Frederiksen K, van Zijl PC, et al. Brain white matter anatomy of tumor patients evaluated with diffusion tensor imaging. Ann Neurol 2002;51:377–380.

206. Kamada K, Todo T, Masutani Y, et al. Combined use of tractography-integrated functional neuronavigation and direct fiber stimulation. J Neurosurg 2005;102:664–672.

207. Kinoshita M, Yamada K, Hashimoto N, et al. Fiber-tracking does not accurately es-

timate size of fiber bundle in pathological condition: initial neurosurgical experience using neuronavigation and subcortical white matter stimulation. Neuroimage 2005;25:424–429.

208. Yu CS, Li KC, Xuan Y, Ji XM, Qin W. Diffusion tensor tractography in patients with cerebral tumors: a helpful technique for neurosurgical planning and postoperative assessment. Eur J Radiol 2005;56:197–204.

209. Laundre BJ, Jellison BJ, Badie B, Alexander AL, Field AS. Diffusion tensor imaging of the corticospinal tract before and after mass resection as correlated with clinical motor findings: preliminary data. AJNR Am J Neuroradiol 2005;26:791–796.

210. Nimsky C, Ganslandt O, Hastreiter P, et al. Intraoperative diffusion-tensor MR imaging: shifting of white matter tracts during neurosurgical procedures—initial experience. Radiology 2005;234:218–225.

211. Nimsky C, Ganslandt O, Hastreiter P, et al. Preoperative and intraoperative diffusion tensor imaging-based fiber tracking in glioma surgery. Neurosurgery 2005;56:130–137.

212. Maruyama K, Kamada K, Shin M, et al. Integration of three-dimensional corticospinal tractography into treatment planning for gamma knife surgery. J Neurosurg 2005;102:673–677.

213. Henry RG, Berman JI, Nagarajan SS, Mukherjee P, Berger MS. Subcortical pathways serving cortical language sites: initial experience with diffusion tensor imaging fiber tracking combined with intraoperative language mapping. Neuroimage 2004;21:616–622.

214. Kamada K, Todo T, Morita A, et al. Functional monitoring for visual pathway using real-time visual evoked potentials and optic-radiation tractography. Neurosurgery 2005;57:121–127.

215. Powell HW, Parker GJ, Alexander DC, et al. MR tractography predicts visual field defects following temporal lobe resection. Neurology 2005;65:596–599.

216. Kamada K, Sawamura Y, Takeuchi F, et al. Functional identification of the primary motor area by corticospinal tractography. Neurosurgery 2005;56:98–109.

217. Coenen VA, Krings T, Axer H, et al. Intraoperative three-dimensional visualization of the pyramidal tract in a neuronavigation system (PTV) reliably predicts true position of principal motor pathways. Surg Neurol 2003;60:381–390.

218. Evans AC. The NIH MRI study of normal brain development. Neuroimage 2006;30:184–202.

219. Sporns O, Tononi G, Kotter R. The human connectome: a structural description of the human brain. PLoS Comput Biol 2005;1:e42.

Radiology 2007

This is your reprint order form or pro forma invoice

(Please keep a copy of this document for your records.)

Reprint order forms and purchase orders or prepayments must be received 72 hours after receipt of form either by mail or by fax at 410-820-9765. It is the policy of Cadmus Reprints to issue one invoice per order. **Please print clearly**.

Author Name _____
Title of Article _____
Issue of Journal_____ Reprint # _____ Publication Date _____
Number of Pages_____ KB # _____ Symbol Radiology
Color in Article? Yes / No (Please Circle)

Please include the journal name and reprint number or manuscript number on your purchase order or other correspondence.

Order and Shipping Information

Reprint Costs (Please see page 2 of 2 for reprint costs/fees.)

_____ Number of reprints ordered $_____
_____ Number of color reprints ordered $_____
_____ Number of covers ordered $_____
Subtotal $_____
Taxes $_____

(*Add appropriate sales tax for Virginia, Maryland, Pennsylvania, and the District of Columbia or Canadian GST to the reprints if your order is to be shipped to these locations*.)

First address included, add $32 for each additional shipping address $_____

TOTAL $_____

Shipping Address (cannot ship to a P.O. Box) Please Print Clearly

Name _____
Institution _____
Street _____
City _____ State _____ Zip _____
Country _____
Quantity_____ Fax _____
Phone: Day _____ Evening _____
E-mail Address _____

Additional Shipping Address* (cannot ship to a P.O. Box)

Name _____
Institution _____
Street _____
City _____ State _____ Zip _____
Country _____
Quantity _____ Fax _____
Phone: Day _____ Evening _____
E-mail Address _____

** Add $32 for each additional shipping address*

Payment and Credit Card Details

Enclosed: Personal Check _____
Credit Card Payment Details _____
Checks must be paid in U.S. dollars and drawn on a U.S. Bank.

Credit Card: __ VISA __ Am. Exp. __ MasterCard
Card Number _____
Expiration Date_____
Signature: _____

Please send your order form and prepayment made payable to:

Cadmus Reprints
P.O. Box 751903
Charlotte, NC 28275-1903

Note: Do not send express packages to this location, PO Box.
FEIN #:541274108

Invoice or Credit Card Information

Invoice Address Please Print Clearly
Please complete Invoice address as it appears on credit card statement

Name _____
Institution _____
Department _____
Street _____
City _____ State _____ Zip _____
Country _____
Phone _____ Fax _____
E-mail Address _____

Cadmus will process credit cards and *Cadmus Journal Services* will appear on the credit card statement.

If you don't mail your order form, you may fax it to 410-820-9765 with your credit card information.

Signature _____ Date _____
Signature is required. By signing this form, the author agrees to accept the responsibility for the payment of reprints and/or all charges described in this document.

RB-9/22/06

Radiology 2007

Black and White Reprint Prices

Domestic (USA only)						
# of Pages	50	100	200	300	400	500
1-4	$213	$228	$260	$278	$295	$313
5-8	$338	$373	$420	$453	$495	$530
9-12	$450	$500	$575	$635	$693	$755
13-16	$555	$623	$728	$805	$888	$965
17-20	$673	$753	$883	$990	$1,085	$1,185
21-24	$785	$880	$1,040	$1,165	$1,285	$1,413
25-28	$895	$1,010	$1,208	$1,350	$1,498	$1,638
29-32	$1,008	$1,143	$1,363	$1,525	$1,698	$1,865
Covers	$95	$118	$218	$320	$428	$530

International (includes Canada and Mexico)						
# of Pages	50	100	200	300	400	500
1-4	$263	$275	$330	$385	$430	$485
5-8	$415	$443	$555	$650	$753	$850
9-12	$563	$608	$773	$930	$1,070	$1,228
13-16	$698	$760	$988	$1,185	$1,388	$1,585
17-20	$848	$925	$1,203	$1,463	$1,705	$1,950
21-24	$985	$1,080	$1,420	$1,725	$2,025	$2,325
25-28	$1,135	$1,248	$1,640	$1,990	$2,350	$2,698
29-32	$1,273	$1,403	$1,863	$2,265	$2,673	$3,075
Covers	$148	$168	$308	$463	$615	$768

Minimum order is 50 copies. For orders larger than 500 copies, please consult Cadmus Reprints at 800-407-9190.

Reprint Cover

Cover prices are listed above. The cover will include the publication title, article title, and author name in black.

Shipping

Shipping costs are included in the reprint prices. Domestic orders are shipped via UPS Ground service. Foreign orders are shipped via a proof of delivery air service.

Multiple Shipments

Orders can be shipped to more than one location. Please be aware that it will cost $32 for each additional location.

Delivery

Your order will be shipped within 2 weeks of the journal print date. Allow extra time for delivery.

Color Reprint Prices

Domestic (USA only)						
# of Pages	50	100	200	300	400	500
1-4	$218	$233	$343	$460	$579	$697
5-8	$343	$388	$584	$825	$1,069	$1,311
9-12	$471	$503	$828	$1,196	$1,563	$1,935
13-16	$601	$633	$1,073	$1,562	$2,058	$2,547
17-20	$738	$767	$1,319	$1,940	$2,550	$3,164
21-24	$872	$899	$1,564	$2,308	$3,045	$3,790
25-28	$1,004	$1,035	$1,820	$2,678	$3,545	$4,403
29-32	$1,140	$1,173	$2,063	$3,048	$4,040	$5,028
Covers	$95	$118	$218	$320	$428	$530

International (includes Canada and Mexico))						
# of Pages	50	100	200	300	400	500
1-4	$268	$280	$412	$568	$715	$871
5-8	$419	$457	$720	$1,022	$1,328	$1,633
9-12	$583	$610	$1,025	$1,492	$1,941	$2,407
13-16	$742	$770	$1,333	$1,943	$2,556	$3,167
17-20	$913	$941	$1,641	$2,412	$3,169	$3,929
21-24	$1,072	$1,100	$1,946	$2,867	$3,785	$4,703
25-28	$1,246	$1,274	$2,254	$3,318	$4,398	$5,463
29-32	$1,405	$1,433	$2,561	$3,788	$5,014	$6,237
Covers	$148	$168	$308	$463	$615	$768

Tax Due

Residents of Virginia, Maryland, Pennsylvania, and the District of Columbia are required to add the appropriate sales tax to each reprint order. For orders shipped to Canada, please add 7% Canadian GST unless exemption is claimed.

Ordering

Reprint order forms and purchase order or prepayment is required to process your order. Please reference journal name and reprint number or manuscript number on any correspondence. You may use the reverse side of this form as a proforma invoice. Please return your order form and prepayment to:

Cadmus Reprints
P.O. Box 751903
Charlotte, NC 28275-1903

Note: Do not send express packages to this location, PO Box.
FEIN #:541274108

Please direct all inquiries to:

Rose A. Baynard
800-407-9190 (toll free number)
410-819-3966 (direct number)
410-820-9765 (FAX number)
baynardr@cadmus.com (e-mail)

Reprint Order Forms and purchase order or prepayments must be received 72 hours after receipt of form.